Journal of Human Evolution 106 (2017) 133–153

Contents lists available at ScienceDirect

Journal of Human Evolution

journal homepage: www.elsevier.com/locate/jhevol

New cranium of the endemic Caribbean platyrrhine, *Antillothrix bernensis*, from La Altagracia Province, Dominican Republic

Lauren B. Halenar [a, b, *], Siobhán B. Cooke [b, c], Alfred L. Rosenberger [d, e, f], Renato Rímoli [g, h]

[a] Department of Biology, Farmingdale State College (SUNY), 2350 Broadhollow Road, Farmingdale, NY 11735, USA
[b] New York Consortium in Evolutionary Primatology Morphometrics Group (NMG), USA
[c] Center for Functional Anatomy and Evolution, Johns Hopkins University School of Medicine, 1830 E Monument Street, Room 305A, Baltimore, MD 21205, USA
[d] Department of Anthropology and Archaeology, Brooklyn College, City University of New York, 2900 Bedford Avenue, Brooklyn, NY 11210, USA
[e] New York Consortium in Evolutionary Primatology (NYCEP), Department of Anthropology, The Graduate Center, City University of New York, 365 Fifth Avenue, New York, NY 10016, USA
[f] Department of Mammalogy, American Museum of Natural History, 79th St at Central Park West, New York, NY 10024, USA
[g] Department of Biology, Universidad Autónoma de Santo Domingo (UASD), Ciudad Universitária, Santo Domingo, Dominican Republic
[h] Museo del Hombre Dominicano, Santo Domingo, Dominican Republic

ARTICLE INFO

Article history:
Received 20 February 2016
Accepted 12 February 2017

Keywords:
Antillothrix bernensis
Platyrrhini
Caribbean primates
Three-dimensional geometric morphometrics
Primate evolution
Greater Antilles

ABSTRACT

Recent paleontological collection in submerged caves in the eastern Dominican Republic has yielded new specimens of *Antillothrix bernensis*. Here we describe a complete cranium of an adult individual (MHD 20) and provide phenetic comparisons to other endemic Caribbean taxa and extant mainland platyrrhines using three-dimensional geometric morphometric methods (3DGM). Qualitative and quantitative comparisons support conclusions based on other recently described fossil material: *Antillothrix* has a dentition lacking clear dietary specialization, an elongated brain case with strong temporal lines, and a vertically oriented nuchal plane. MHD 20 shares a combination of traits with a previously published subadult specimen (MHD 01) including a deep depression at glabella, dorsoventrally elongated orbits, and a relatively large face. This shared morphology reinforces the taxonomic affinity of the two specimens, with differences between the two likely reflecting the younger ontogenetic age of MHD 01.

Comparisons to the extant platyrrhines paint a complicated picture as the results of between-group principal components analyses (bgPCA) indicate that *Antillothrix* does not share a suite of morphological features exclusively with any one genus. Depending on which bgPC axes are visualized, and which subset of landmarks is included (i.e., only those describing the shape of the face/palate for inclusion of *Xenothrix*), MHD 20 is most similar in shape to the atelids, *Alouatta, Lagothrix,* and *Brachyteles*, or an otherwise "empty" region of shape space. It groups neither with *Cebus* nor *Callicebus*, two taxa that *Antillothrix* has been associated with in previous studies based on much less complete material. The *Antillothrix* cranium does not exhibit any of the derived characters classically used to diagnose or define any single clade; rather its morphology shares features with multiple platyrrhine groups. This is consistent with the interpretation that *Antillothrix* preserves a primitive morphology, which accords with the hypothesis positing an early arrival of platyrrhines in the Caribbean.

1. Introduction

There are four genera and five species of platyrrhine primates that were endemic to the islands of the Greater Antilles: *Antillothrix bernensis* from Hispaniola (Rímoli, 1977; MacPhee et al., 1995), *Insulacebus toussaintiana* from Haiti (Cooke et al., 2011), *Paralouatta varonai* and *Paralouatta marianae* from Cuba (Rivero and Arredondo, 1991; MacPhee et al., 2003), and *Xenothrix mcgregori* from Jamaica (Williams and Koopman, 1952; Rosenberger, 1977; MacPhee and Horovitz, 2004; MacPhee and Meldrum, 2006) (Fig. 1). The recently named *Insulacebus* is represented by dentognathic remains only (Cooke et al., 2011), though postcranial remains from nearby sites exist (e.g., Tallman and Cooke, 2016). The

* Corresponding author.
E-mail address: lauren.halenar@gmail.com (L.B. Halenar).

http://dx.doi.org/10.1016/j.jhevol.2017.02.002
0047-2484/

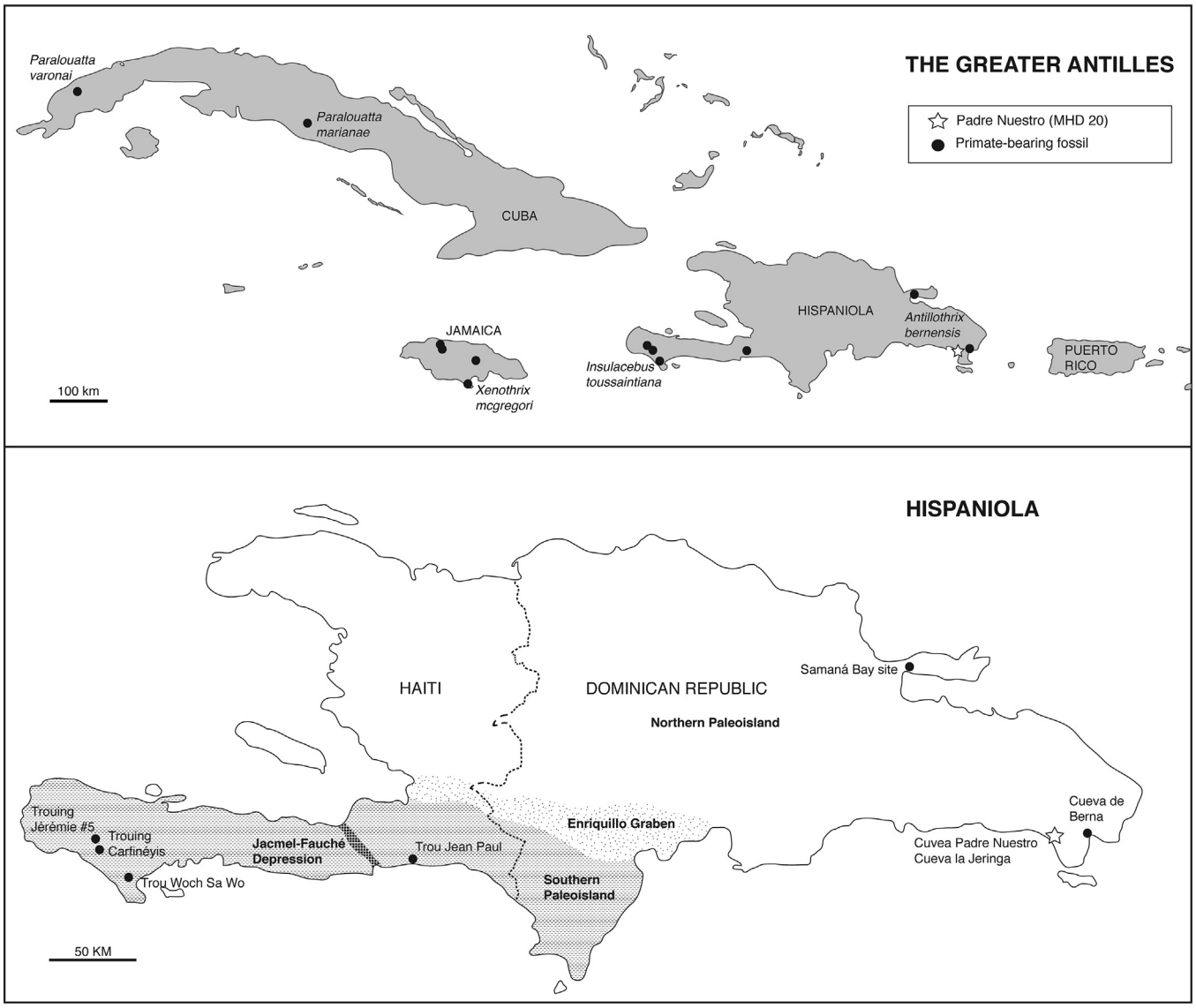

Figure 1. Primate fossil localities across the Caribbean (top). Specific localities known so far from Hispaniola (bottom); white portions of the Hispaniola map indicate the northern paleoisland; the stippled portion represents the Enriquillo Graben; the gray portion indicates the southern paleoisland. Specimens securely identified as *Antillothrix* come from the Dominican Republic.

other three genera include cranial, dental, and postcranial elements in their hypodigms (MacPhee and Horovitz, 2002; MacPhee and Meldrum, 2006; Rosenberger et al., 2011).

Several of these species are only recently extinct, though evidence exists that the endemic primates entered the islands as early as the Early Miocene (*P. marianae;* MacPhee et al., 2003). The latest date of appearance on the islands is for the Jamaican primate *Xenothrix,* which disappears during the Holocene and may have overlapped with the first humans to colonize the island (MacPhee and Fleagle, 1991; McFarlane et al., 2002; Cooke et al., in press). Given their long tenure isolated on the Greater Antilles, these species have been difficult to place phylogenetically. Each of them presents a mixture of derived and primitive features making their relationships – both with each other and with mainland forms – a matter of some debate. The major arguments around their relationships have centered on: 1) whether they are part of a monophyletic pitheciid Greater Antillean radiation (e.g., MacPhee et al., 1995; Horovitz and MacPhee, 1999; MacPhee and Horovitz, 2004), 2) whether the genera are related to several different mainland clades (e.g., Ford and Morgan, 1986; Rosenberger, 2002; Cooke et al., 2011), or alternately, 3) whether they are, collectively, stem platyrrhines falling outside of the extant platyrrhine families (e.g., Kay, 2015). No clear resolution has been achieved on this point to date.

Less work has been completed on their paleobiology, though various studies indicate that they may differ somewhat from mainland forms. *P. varonai* has been suggested to be semiterrestrial (MacPhee and Meldrum, 2006) – a unique locomotor pattern among platyrrhines, extant or extinct. Locomotor repertoire reconstructions for the other species have varied with *Xenothrix* largely being reconstructed as a deliberate and slow arboreal quadruped or climber (MacPhee and Fleagle, 1991; MacPhee and Meldrum, 2006), and *Antillothrix* reconstructed as an arboreal quadruped (Cooke and Tallman, 2012; Tallman and Cooke, 2016). Interestingly, there is a commonality in that all the Greater Antillean primates have robust postcrania in comparison with mainland extant species (e.g., MacPhee and Horovitz, 2004; Rosenberger et al., 2011; Cooke and Tallman, 2012; Tallman and Cooke, 2016). They also occupy a body size niche, between approximately three and 7 kg, which straddles the divide between the smaller cebids

and pitheciids and the larger atelids on the mainland (Perry et al., 2015). Dental morphology indicates few adaptations showing dietary specialization – with the exception of *Xenothrix*, which has a reduced dental formula and extremely low-cusped molars quite distinct from any living forms (Rosenberger, 1977; Horovitz and MacPhee, 1999; MacPhee and Horovitz, 2004; Cooke, 2011).

Until recently, *Antillothrix* was the least known of these platyrrhines. The type maxilla of *Antillothrix* (CENDIA-1[1]; Fig. 2) was described by Rímoli (1977) as a new species of squirrel monkey, *Saimiri bernensis*, owing to similarities in dental morphology between it and the living genus. Shortly after this discovery, a fragmentary mandible with teeth (UF 28038 – now lost) was recovered in western Haiti (MacPhee and Woods, 1982). In addition to these dento-gnathic remains, a distal tibia (USNM 254682) found in 1928 by Gerrit S. Miller (1929) was also ultimately assigned to this taxon (Rosenberger, 1978; MacPhee and Woods, 1982; Hershkovitz, 1988; Rosenberger et al., 2015a). In 1995, with morphological differences between the Hispaniolan material and living *Saimiri* now readily apparent (see Rosenberger, 1978), MacPhee and colleagues (MacPhee et al., 1995) named a new genus: *Antillothrix*. Over the last eight years, the originally small number of fossils attributed to this Hispaniolan primate has grown considerably, improving our knowledge of its morphology. There are now three well-preserved crania: one subadult, MHD 01 (Rosenberger et al., 2011), and two adults, PN-09-01 (Kay et al., 2011b) and MHD 20. The last is described here for the first time here. There is also a complete mandible from MHD 01 (Rosenberger et al., 2013) and many as yet undescribed postcranial specimens.

The adult MHD 20 cranium of *A. bernensis* is one of only a few complete, undistorted platyrrhine crania[2] free of surrounding matrix and with many teeth in situ, making it important for evaluating cranial morphology in extinct platyrrhine primates generally. In this study, we use 3DGM analyses and standard linear measurements to address the following research questions pertinent to gaining a more complete understanding of its paleobiology, evolutionary relationships, and morphology:

1) How does the *Antillothrix* cranial shape fit within the range of shape variation observed in extinct and extant platyrrhine primates?
2) Using cranial centroid size derived from *x,y,z* coordinate landmarks, what is the predicted body mass of *Antillothrix*? How does this mass compare with previous postcranial and dental estimates?
3) Finally, since previous cladistic analyses were completed when much less was known about the cranial morphology of *Antillothrix*, how does the morphology of the MHD 20 cranium fill in the gaps in phylogenetic matrices for characters proposed to be most relevant to the evolutionary relationships of the Caribbean primates?

[1] Abbreviations: CENDIA = Centro Dominicano de Investigaciones Anthropologicas, Santo Domingo, Dominican Republic; UF = Florida Museum of Natural History, Gainesville; USNM = United States National Museum of Natural History, Washington, DC; MHD = Museo del Hombre Dominicano, Santo Domingo, Dominican Republic; PN = Padre Nuestro; AMNH = American Museum of Natural History, New York; MNHN = Museo Nacional de Historia Natural, La Habana, Cuba; MCL = Museu de Ciencias Naturais PUC Minas Gerais, Belo Horizonte, Brazil.

[2] Other complete and nearly complete largely undistorted platyrrhine crania include: *Antillothrix bernensis,* subadult, MHD 01; *Caipora bambuiorum,* IGC-UFMG 05; *Cartelles coimbrafilhoi*, IGC-UFMG 06; *Chilecebus carrascoensis,* SGOPV 3213; *Homunculus patagonicus*, MPM-PV 3501; MPM-PV 3502; *Killikaike blakei*,face only, MPM-PV 5000; *Paralouatta varonai*, MNHN V194. Two additional crania are known that are nearly complete, but distorted: *Tremacebus harringtoni* and *Dolichocebus gaimanensis*.

Figure 2. Type specimen of *Antillothrix bernensis* (CENDIA-1) from Cueva de Berna (left) and MHD 20 from Padre Nuestro (right), showing comparable dentition preserved in the two specimens (from bottom to top, occlusal view of M^2, M^1, P^4).

2. Discovery and taphonomic context

The MHD 20 cranium (Figs. 2–4; Supplementary Online Material [SOM] Fig. S1) was discovered submerged in the Padre Nuestro cave on September 26, 2012 by Phillip Lehman. Padre Nuestro is also the source of another adult cranial specimen of *A. bernensis* (PN-09-01; Kay et al., 2011b, Fig. 4), which was discovered in 2009. La Jeringa, a submerged cave site located about 500 m away, was the source of the subadult cranium, mandible, and associated postcranial remains (MHD 01; Rosenberger et al., 2011, 2013, Fig. 4), which were also recovered in 2009. Both cave sites are in Parque del Este, La Altagracia Province in the southeastern Dominican Republic (Fig. 1). The type site for *A. bernensis,* Cueva de Berna, is found just outside the park boundary approximately 22 km east of the Padre Nuestro and La Jeringa sites near Boca de Yuma.

Padre Nuestro was once a dry cave complex as evidenced by the formation of speleothems, but currently is water-filled – potentially as a result of sea-level rise after the Last Glacial Maximum around 22,000–19,000 calendar years before present (Blanchon and Shaw, 1995; Yokoyama et al., 2000). The present-day cave mouth allows entrance into a large cavern that has been the source of many vertebrate remains – including mammals, birds, and reptiles. The Padre Nuestro cave system is particularly rich in mammalian fauna, many extinct, including three pilosans (*Parocnus serus, Acratocnus ye, Neocnus dousman*), four rodents (*Isolobodon portoricensis, Brotomys voratus, Plagiodontia aedium*, *Hexolobodon phenax*), three bats (*Phyllonycteris poeyi*, *Erophylla bombifrons, Mormoops blainvillei*), and four lipotyphlans (*Solenodon paradoxus, Nesophontes paramicrus, N. hypomicrus, N. zamicrus*). The MHD 20 cranium was located in a shallower area that extends out of the entry cavern and contains debris and some of the other faunal remains listed above. Various "rooms" deeper in the cave have also yielded *Antillothrix* specimens. Divers with the Dominican Republic Speleological Society (DRSS) are currently working on a detailed map of the caves (Z. Klukkert, pers. comm.); a preliminary map can be found on their website (www.dr-ss.com).

Dating fossil remains from submerged caves is notoriously difficult; however, a date of approximately 1.3 Ma was obtained using uranium series methods on samples from speleothem encasing one of the recently discovered tibiae attributed to *Antillothrix* from Padre Nuestro (Rosenberger et al., 2015a). This date is the oldest known for material associated with a Hispaniolan fossil mammal. Other dates from Hispaniolan sites containing primate remains are Holocene in age (e.g., Rímoli, 1977; MacPhee and Woods, 1982), though these dates were inferred from associated material and not from the specimens themselves, leaving open the

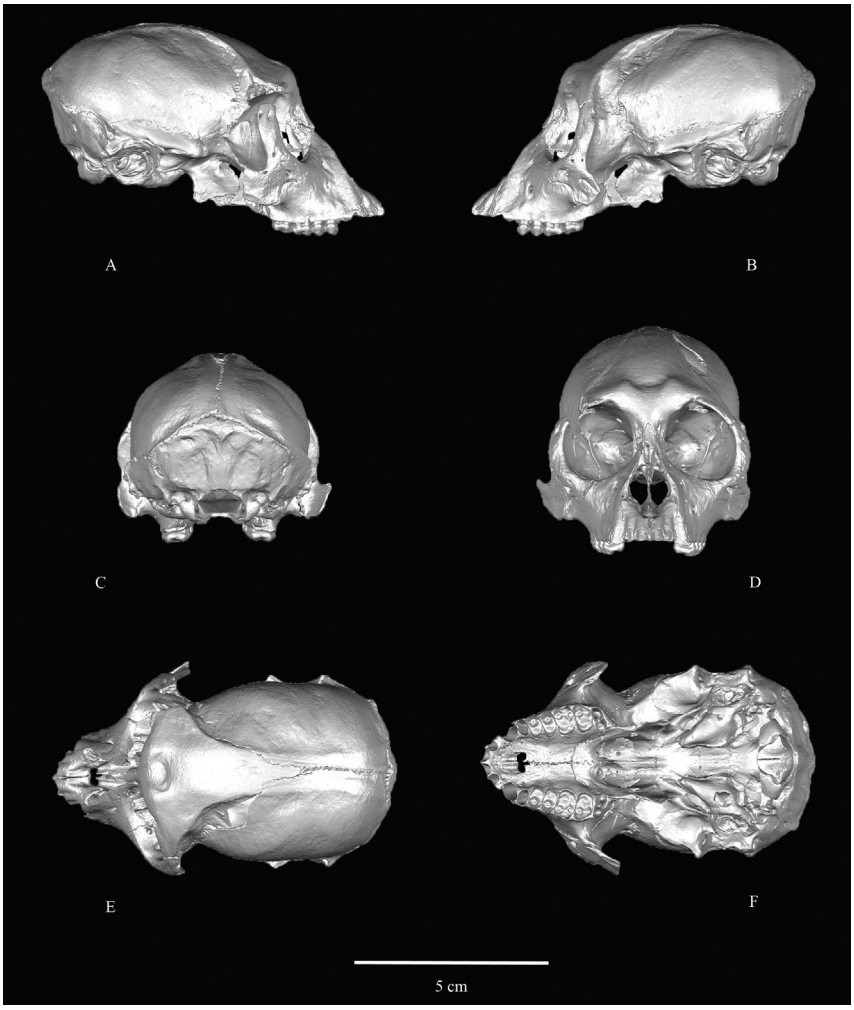

Figure 3. μCT reconstruction of the cranium of MHD 20 in right lateral (A), left lateral (B), posterior (C), frontal (D), superior (E), and inferior (F) views.

possibility that the specimens are, in fact, older. Given the depositional environment at these sites, it is unlikely that the *Antillothrix* specimens are substantially older than the surrounding material, however. Regardless, the paleontological record on Hispaniola suggests that *Antillothrix* had a relatively long tenure on the island.

3. Materials and methods

Standard linear measurements were taken by L.B.H. using digital calipers on the MHD 20 cranium, the *P. varonai* cranium (cast of MNHN V194, type specimen), and a partial face and palate of *X. mcgregori* (AMNH 268006). The same measurements were taken using Geomagic Studio 2014 on a reconstruction of the PN-09-01 *Antillothrix* cranium made from a CT scan (downloaded from MorphoSource: http://doi.org/10.17602/M2/M9349). These were compared to published values for MHD 01 (Rosenberger et al., 2011) and a sample of extant platyrrhines (Sears et al., 2008) (Table 1). The measurements include: braincase length (BCL), braincase width (BCW), skull length (SL), palate length (PalL), palate width (PalW), interorbital breadth (Interorb), orbital aperture width (OrbW), orbital aperture height (OrbH), foramen magnum length (FMH), foramen magnum width (FMW), facial height (FacialH), an occipital chord from lambda to opisthion (Occ chord), frontal chord from bregma to nasion (Front chord), parietal chord from bregma to lambda (Par chord), and temporal chord from bregma to asterion (Temp chord) (Fig. 5). As previous phylogenetic analyses have included relative canine to premolar size as an informative character (e.g., Horovitz and MacPhee, 1999; MacPhee and Horovitz, 2004), buccolingual width was also measured on these teeth in MHD 20 and in a sample of other fossil and extant specimens by S.B.C. (Table 2). Endocranial volume was also measured for MHD 20 and MHD 01 by pouring glass beads into the cranial cavity through the foramen magnum and then transferring them into a graduated cylinder. These values were then compared to endocranial volumes for extant platyrrhine taxa taken from Isler et al. (2008) (Table 1).

In an effort to quantify and more easily visualize comparable morphology among MHD 20, other Greater Antillean and mainland fossil taxa, and extant platyrrhines, three dimensional geometric morphometric techniques were also employed. The extant sample used for these analyses consists of surface scans of 521 adult wild-shot individuals from the Mammalogy collections of the American Museum of Natural History (AMNH) in New York and the National Museum of Natural History (NMNH) in Washington, DC. The sample includes at least one genus of all the major non-callitrichine platyrrhine clades and the more speciose genera are represented by multiple species (Table 3). For most species, approximately 20 individuals total, including both males and females, were sampled.

Scans of the NMNH specimens were downloaded from the National Museum's publicly available online database of 3D primate specimens (http://humanorigins.si.edu/evidence/3d-collection/primate), which are reconstructed from CT scans. All of the extant

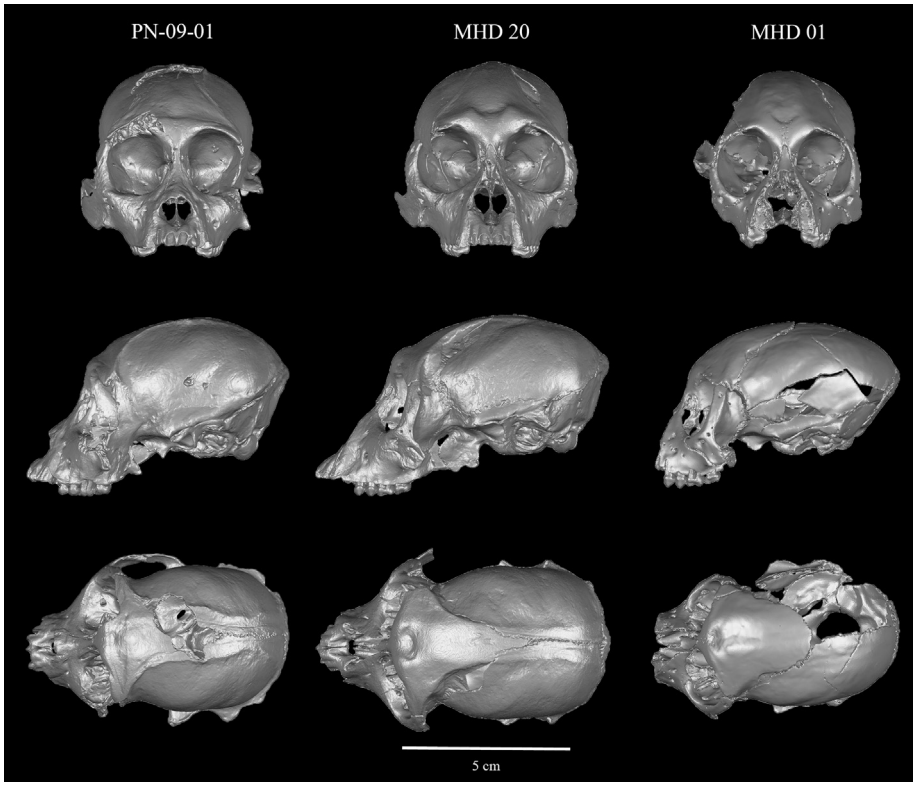

Figure 4. μCT reconstructions of the PN-09-01 cranium (left), adult MHD 20 cranium (center), and the subadult MHD 01 cranium (right) in frontal (top), left lateral (middle), and superior (bottom) views. The three crania share a very similar neurocranial profile in lateral view in particular, but there are several differences between the two adult crania that should be noted such as the shape of the orbits, the path of the temporal lines, length and orientation of the premaxilla, and the lack of the deep depression at glabella and raised superciliary bosses in PN-09-01 that are shared between MHD 20 and MHD 01. See main text for further discussion.

Table 1
Cranial measurements (in mm).

Taxon	n[a]	BCL	BCW	SL	PalL	PalW	Interorb	OrbW	OrbH	FMH	FMW	FacialH	Occ chord	Front chord	Par chord	Temp chord	ECV[b] (mL)	Body mass (kg)
MHD 20	1	**50.34**	**45.13**	**90.63**	**29.14**	**14.66**	**4.59**	**18.89**	**20.36**	**12.41**	**12.35**	**38.15**	**20.29**	**48.64**	**21.10**	**33.64**	**39**	**3.2–3.3**[c]
MHD 01[d]	1	**60.92**	**42.51**	78.75	**17.12**	**12.44**	6.62	18.50	20.50	**14.22**	**11.29**	**25.14**	**19.68**	**38.10**	**33.50**	**36.80**	**38**	4–6
PN-09-01[e]	1	**51.11**	**44.99**	**82.71**	**25.16**	**12.70**	**6.19**	**18.96**	**20.18**	**12.09**	**11.62**	**27.15**	**18.73**	**42.67**	**25.64**	**32.31**	41	3.3
Pa. varonai[f]	1	**67.46**	**50.74**	**115.74**	**32.87**	**17.95**	**7.50**	**22.12**	**29.29**	**11.70**	**12.93**		**28.47**		**30.24**	**40.21**	45	9.1–10.1
X. mcgregori[g]	1				**25.67**	**10.56**												5.8–6.5
At. geoffroyi	10	68.92	64.23	111.7	34.83	21.24	**8.46**	27.38	**22.44**	18.15	16.29	40.98	29.11	65.99	47.41	51.36	105	7.5
B. arachnoides	2	75.62	62.91	111.51	36.65	36.30	**10.27**	21.53	**23.81**	16.63	14.94	37.32	22.36	53.00	45.29	53.32	117	8.8
La. lagotricha	10	65.38	65.57	116.33	33.84	21.76	**7.01**	29.05	**22.73**	15.35	14.65	38.35	24.33	60.51	38.4	52.68	97	7.2
Al. caraya	8	49.00	50.21	105.38	42.04	24.52	**10.55**	25.17	**21.39**	12.27	13.47	39.03	19.73	44.34	32.23	37.78	53	5.4
Sai. sciureus	10	41.35	39.08	69.94	18.38	11.70	**3.50**	17.00	**14.60**	8.49	9.47	21.04	20.71	36.15	31.54	35.23	24	0.8
Ce. apella	10	62.37	58.49	104.72	35.16	20.39	**5.40**	24.63	**20.69**	15.00	24.54	38.60	24.99	61.50	30.27	46.45	67	2.9
Callic. moloch	10	37.43	37.58	69.77	21.00	12.65		18.31		7.43	9.67	23.17	15.80	32.49	30.19	29.90	18	0.9
Ao. vociferans	10	33.90	37.02	65.28	18.76	13.24		23.34		9.16	9.43	22.52	14.55	33.11	29.64	30.93		
Pi. pithecia	10	45.85	45.50	84.31	27.29	13.18	**5.59**	20.09	**16.68**	9.78	11.99	28.99	20.16	43.68	27.23	35.91	32	1.8
Ch. satanas	10	53.73	55.80	96.16	28.44	16.48	**4.75**	24.56	**19.67**	12.20	13.04	34.40	22.79	40.94	39.18	46.33	57	2.7
Cac. calvus	10	64.77	53.60	96.36	24.54	26.93	**5.30**	18.92	**22.36**	12.90	13.28	32.62	24.24	44.09	42.38	46.92	76	3.2
Le. rosalia	10	34.05	30.26	59.21	19.22	12.03		12.94		6.55	7.82	18.86	14.56	28.69	26.61	27.40	13	0.6
Callim. goeldi	11	37.37	29.76	51.94	15.20	18.73		12.52		7.12	7.68	15.24	12.74	28.38	26.71	25.17	11	0.5
Callit. jacchus	10	28.00	27.24	49.01	15.49	9.12		11.16		6.41	6.95	15.45	11.12	26.13	20.56	22.44	7	0.3
Callit. pygmaea	10	26.38	20.80	34.44	8.70	10.95		9.06		6.01	5.62	9.58	6.82	19.62	17.49	17.50	4	0.1
Sag. mystax	10	33.13	30.75	58.41	18.12	11.70		13.15		7.42	7.92	17.71	12.34	26.22	27.79	26.63	11	0.6

[a] Sample sizes, measurement definitions, and data for extant taxa are from Sears et al. (2008). See Materials and methods section in the main text here for acronym definitions. Measurements in bold for fossils and extant taxa were taken by L.B.H. with sample sizes for extant taxa matching those in Table 3 and measurement definitions from Rosenberger et al. (2011).

[b] Endocranial volume and body mass for extant taxa are from Isler et al. (2008).

[c] Body mass as estimated from cranial centroid size in this paper (see Materials and methods section).

[d] Non-bold measurements are from Rosenberger et al. (2011).

[e] Measurements on PN-09-01 were taken using Geomagic Studio on a reconstruction of the specimen from a CT scan. Endocranial volume and body mass estimate from Allen et al. (2012).

[f] Endocranial volume reconstructed by S.B.C. from CT scan of the original specimen. Body mass estimate from MacPhee and Meldrum (2006).

[g] Body mass estimate from MacPhee and Meldrum (2006).

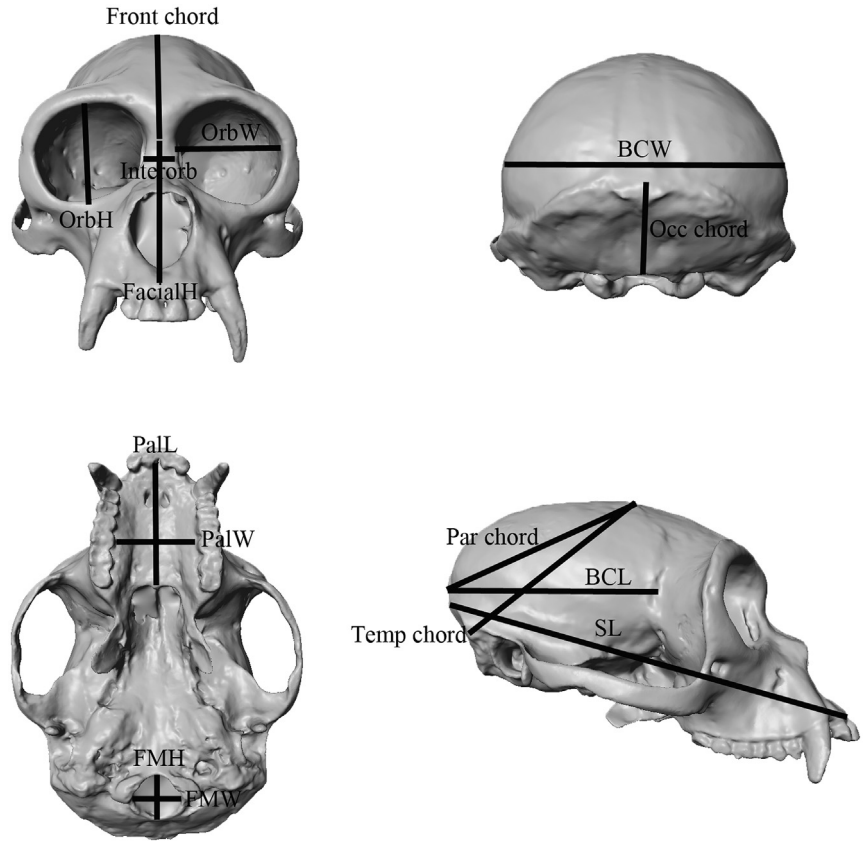

Figure 5. Surface scan of the cranium of a male *Lagothrix* showing the definitions of the linear measurements found in Table 1. BCL = braincase length, BCW = braincase width, SL = skull length, PalL = palate length, PalW = palate width, Interorb = interorbital breadth, OrbW = orbital aperture width, OrbH = orbital aperture height, FMH = foramen magnum length, FMW = foramen magnum width, FacialH = facial height, Occ chord = lambda to opisthion, Front chord = bregma to nasion, Par chord = bregma to lambda, Temp chord = bregma to asterion.

AMNH specimens were scanned with a NextEngine desktop laser surface scanner using HD resolution, except for six of the *Cebus* and two of the *Chiropotes* individuals which were CT scanned using the GE Phoenix v/tome/x s 240 micro-CT scanner in the Microscopy and Imaging Facility at the AMNH. For the NextEngine scans, each specimen was scanned in three different orientations (sitting on its basicranium, "standing up" on its occipital, and laying on its side on the zygomatic arch) so that the laser scanner would capture as

Table 2a
Canine and premolar measurements of selected platyrrhine taxa (in mm).

Taxon	*n*	Lower p4 BL width	Lower c BL width	Lc/p4	Upper P4 BL width	Upper C BL width	UC/P4
Alouatta palliata	5 M, 4 F	5.38	5.79	1.08	7.25	5.83	0.80
Lagothrix lagotricha	6 M, 4 F	3.92	5.53	1.41	5.67	6.02	1.06
Ateles geoffroyi vellerosus	3 M, 7 F	3.73	4.60	1.23	5.14	4.77	0.93
Brachyteles arachnoides	5 M, 5 F	4.47	5.34	1.20	7.21	5.68	0.79
Cebus capucinus	5 M, 5 F	4.68	6.11	1.31	5.63	5.75	1.02
Saimiri boliviensis	5 M, 5 F	1.91	2.69	1.41	3.53	2.78	0.79
Aotus vociferans	3 M, 4 F	1.97	2.20	1.12	3.19	2.41	0.75
Callicebus discolor	6 M, 3 F, 1 UNK	2.41	2.45	1.01	3.31	2.60	0.79
Pithecia irrorata irrorata	5 M, 3 F	3.40	5.04	1.48	4.40	4.67	1.06
Cacajao melanocephalus	4 M, 4 F	3.58	6.10	1.70	4.75	5.15	1.09
Chiropotes satanas	5 M, 5 F	3.52	6.01	1.71	4.69	5.37	1.14
Antillothrix bernensis (MHD 01)	1	4.29	5.58	1.30	6.69	4.22	0.63
Antillothrix bernensis (MHD 21)	1	4.00	4.93	1.23			
Antillothrix bernensis (MHD 20)	1				6.23	4.60	0.74
Antillothrix bernensis (MHD 13)	1				6.34	4.24	0.67
Antillothrix bernensis (CENDIA-1)	1				6.73	5.34	0.79
Antillothrix bernensis (PN-09-01)[a]	1				6.03	4.28	0.71
Paralouatta varonai (V195)	1	5.90	4.10	0.69			
Xenothrix mcgregori (AMNH 148198)[b]	1	4.63	3.31				
Xenothrix mcgregori (AMNH 268006)					6.10	4.30	0.70

[a] measurements taken in Geomagic Studio on a surface reconstructed from a CT scan.
[b] measurements for both *Xenothrix* specimens (AMNH 148198, AMNH 268006) from MacPhee and Horovitz (2004).

Table 2b
Upper C/P4 ratio partitioned by sex.

Species	Sex	Upper C/P4
Alouatta palliata	F	0.71
Alouatta palliata	M	0.88
Lagothrix lagotricha	F	0.89
Lagothrix lagotricha	M	1.20
Ateles geoffroyi vellerosus	F	0.94
Ateles geoffroyi vellerosus	M	0.91
Brachyteles arachnoides	F	0.75
Brachyteles arachnoides	M	0.82
Cebus capucinus	F	0.97
Cebus capucinus	M	1.09
Saimiri boliviensis	F	0.72
Saimiri boliviensis	M	0.86
Aotus vociferans	F	0.73
Aotus vociferans	M	0.77
Callicebus discolor	F	0.89
Callicebus discolor	M	0.76
Pithecia irrorata irrorata	F	1.01
Pithecia irrorata irrorata	M	1.09
Cacajao melanocephalus	F	1.00
Cacajao melanocephalus	M	1.17
Chiropotes satanas	F	1.07
Chiropotes satanas	M	1.20

Table 3
Extant comparative sample for three-dimensional geometric morphometric analyses.

Genus	Species	Females	Males	Unknown	TOTAL
Alouatta	*belzebul*	14	21	–	35
Alouatta	*caraya*	9	12	–	21
Alouatta	*guariba*	3	2	–	5
Alouatta	*palliata*	21	26	–	47
Alouatta	*pigra*	3	3	–	6
Alouatta	*seniculus*	29	42	–	71
Ateles	*belzebuth*	14	6	–	20
Ateles	*fusciceps*	2	–	–	2
Ateles	*geoffroyi*	12	15	–	27
Ateles	*paniscus*	11	–	–	11
Brachyteles	*arachnoides*	2	–	2	4
Cacajao	*calvus*	5	6	–	11
Cacajao	*melanocephalus*	2	3	–	5
Callicebus	sp.	9	12	–	21
Callicebus	*torquatus*	11	10	–	21
Cebus	*albifrons*	10	9	–	19
Cebus	*apella*	18	21	–	39
Cebus	*capucinus*	9	11	–	20
Chiropotes	*satanas*	18	16	–	34
Lagothrix	*lagotricha*	20	23	–	43
Pithecia	*monachus*	8	9	–	17
Pithecia	*pithecia*	8	17	–	25
Saimiri	*boliviensis*	8	9	–	17

much of the surface as possible. The three orientations were manually aligned and merged into one solid surface model using Geomagic Studio 2014; all holes were filled in, and the surface was optimized using the Mesh Doctor module.

The fossil sample consists of *A. bernensis* (MHD 20 and PN-09-01 only as MHD 01 is a subadult and missing half of the neurocranium), a partial lower face of *X. mcgregori* (AMNH 268006), and the nearly complete crania of *P. varonai* (MNHN V194) and the Brazilian *Cartelles coimbrafilhoi* (MCL 06). *Cartelles* was included for comparison as it is another Pleistocene-Recent taxon with a mosaic of traits overlapping multiple extant platyrrhine clades. As with *Antillothrix,* several researchers have also suggested that *Cartelles* is a more primitive member of an extant lineage despite its relatively recent geological age (Hartwig and Cartelle, 1996; Halenar, 2012; Halenar and Rosenberger, 2013; Rosenberger et al., 2015b). The scans of *Paralouatta* and *Cartelles* were done on high-fidelity epoxy casts using the NextEngine and the same protocols as for the extant specimens described above. MHD 20 and AMNH 268006 were micro-CT scanned at the AMNH Microscopy and Imaging Facility. Data from these CT scans will be posted on the MorphoSource website (Boyer et al., 2014) and available for download by request. A recent study looking at the amount of error introduced into 3DGM studies when multiple devices are used to collect surface scans found it to be negligible (Shearer et al., 2014); therefore, mixing NextEngine and CT scans in this sample should not affect the results.

Forty-four three-dimensional landmarks (a series of *x,y,z* coordinates that describe the overall shape of a specimen) were collected on these virtual specimens using Landmark Editor (Wiley et al., 2005) by one of us only (L.B.H.) so as to not introduce inter-observer error in landmark placement (Fig. 6; Table 4). The dataset consists of Type I, II and III landmarks (Bookstein, 1991) and was modified from Frost et al. (2003) to describe overall cranial shape as it varies across platyrrhines. Several partial landmark configurations were also used so that the slightly damaged *Paralouatta* and more fragmentary *Xenothrix* specimen could be included in the analyses (Table 4). Once collected, the landmark configurations were aligned using a generalized Procrustes analysis (GPA), which rotates, translates, and scales the landmark map such that the mean sum of squared distances among the points is minimized (O'Higgins and Jones, 1998). This minimizes the influence of absolute size differences within the sample and yields a series of Procrustes-aligned coordinates that describe the shape of each specimen, which can then be statistically analyzed.

In order to more easily visualize the axes of maximum shape variation within the comparative sample and where MHD 20 falls within that shape space, between-group principal components analyses (bgPCA; Mitteroecker and Bookstein, 2011) were conducted using the PAST 3.02a software package (Hammer et al., 2001). Between-group principal components analysis first calculates the mean shape of each user-defined group; here, males and females of each species were defined separately due to the relatively high degree of sexual dimorphism seen in many of the extant taxa. bgPCA then orients the individual specimen variation with respect to those group means. This can lead to a clearer separation between groups than that seen in a standard PCA but without overemphasizing artificial group differences as can happen in a canonical variates analysis (CVA) (Mitteroecker and Bookstein, 2011).

A single fossil specimen is more comparable to the single data point contributed by a species mean shape, but the known range of variation around that mean for an extant taxon is also important to include in the analysis; a bgPCA allows for visualization of both aspects of the comparative data set, thus yielding a more complete picture of phenetic affinities. This range of variation was also visualized by creating histograms showing the distribution of pairwise Procrustes distances within species, between species, and between genera. The distance between the two fossils assigned to *Antillothrix* (MHD 20 and PN-09-01) was then compared to the ranges seen in the extant sample. For all analyses, extant and fossil specimens were analyzed together to produce a single covariance matrix, i.e., the PC scores for the fossil specimens were not back-calculated and added into the morphospace of the extant sample. Shape changes were visualized and wireframes representing the shapes of the extant taxa at the extreme ends of their distribution along each bgPC axis were produced in Morphologika v2.5 (O'Higgins and Jones, 2006).

As a single two-dimensional PCA plot is meant to simplify and compress multidimensional space, the nearest neighbor to a fossil is not always apparent graphically. In other words, the nearest neighbor plotted on a paired set of axes is not necessarily the most similar to the specimen overall. To attempt to circumvent this potential visual confusion, the male and female mean shapes for each species were overlaid with a minimum spanning tree that connects

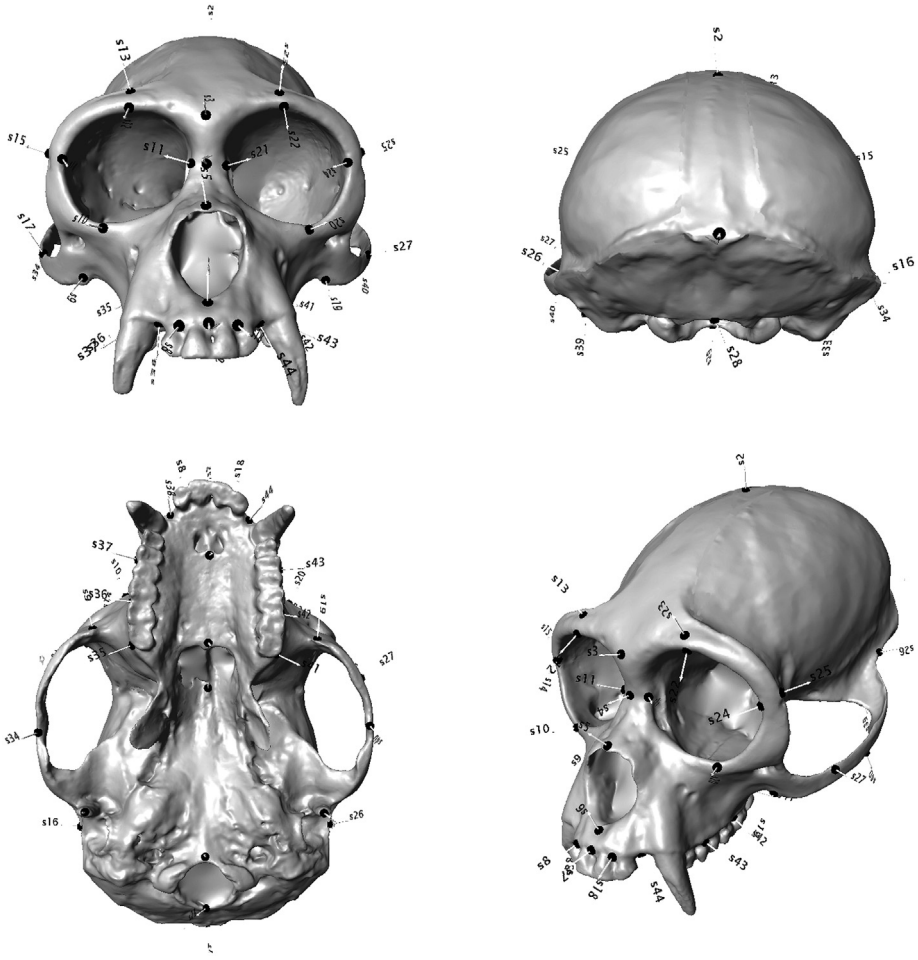

Figure 6. Surface scan of the cranium of a male *Lagothrix* showing the placement of the 44 landmarks used in this study. See Table 4 for the landmark definitions.

all of the shapes with the shortest path based on a Euclidean distance measure (Hammer et al., 2001). While this procedure may make these plots look in some ways like phylogenetic trees, it should be emphasized that this is a purely phenetic analysis. And, while previous studies have shown that phylogeny plays a statistically significant role in driving the variation in cranial shape within platyrrhines (e.g., Perez et al., 2011; Aristide et al., 2015; Bjarnason et al., 2015), this was not explicitly tested in this study.

An estimate of body mass for any fossil taxon is key to understanding crucial aspects of its ecological niche and paleobiology, including diet and locomotion. Previous publications have attempted to estimate body mass for *Antillothrix* using either dental dimensions (e.g., MacPhee and Meldrum, 2006; Rosenberger et al., 2011), dental and cranial dimensions combined (e.g., Allen et al., 2012), or postcranial joint sizes (e.g., Perry et al., 2015). All of these methods may suffer from overestimation as both the molars and joint surfaces of *Antillothrix* seem to be enlarged relative to the size of the mandibles or length of the long bone shafts (Rosenberger et al., 2011). Here, a fourth methodology is developed, using three-dimensional landmarks to calculate the centroid size (the square root of the sum of squared distances of a set of landmarks from their centroid; Bookstein, 1991) of the cranium. Centroid size was then used as the independent variable in a traditional regression-based body mass estimation procedure (see Halenar, 2011; Perry et al., 2015). The natural logarithm of species mean cranial centroid size for many of the taxa in the comparative sample was regressed against the natural logarithm of species mean body mass taken from Isler et al. (2008) using ordinary least squares regression (OLS, Model I) (Table 5). A phylogenetically-corrected least-squares regression (PGLS) approach (Felsenstein, 1985) was also employed using the "caper" package for R (Orme et al., 2010) to control for phylogenetic effects. A consensus tree (phylogram) was generated using 10K trees (Arnold et al., 2010) for the platyrrhines in our sample, which followed the branching topology of Perelman et al. (2011). For the PGLS, log base 10 of the extant species mean cranial centroid size was regressed on the log base 10 of species mean body mass from Isler et al. (2008).

The log-transformation of the independent and dependent variables and subsequent de-transformation of the eventual estimate introduces bias (Smith, 1993) so the Quasi-Maximum Likelihood Estimator [QMLE = exp (MSE/2) where MSE is the residual mean square error of the regression equation; Delson et al., 2000; Jungers et al., 2008] was used as a correction factor. R^2 values and standard error of the estimate (SEE) were calculated to evaluate the statistical strength of the resulting equation. Unfortunately, mean prediction error (MPE) could not be calculated as too few of the extant specimens in the comparative sample had associated known body weights recorded in the AMNH or NMNH catalogs.

4. Results

4.1. Description and comparative anatomy

MHD 20 is a nearly complete cranium, closest in skull length to *Pithecia* or *Cacajao* amongst extant platyrrhines (Table 1). Both zygomatic arches, the tips of the pterygoids, the orbital floors, and

Table 4
Three-dimensional landmark configuration and definitions.

	Landmark	Side	Definition[a]
^1	Inion		Most posterior point of the cranium, when viewed in Frankfurt horizontal
^2	Bregma		Junction of coronal and sagittal sutures
^3	**Glabella**		Most anterior midline point on the frontal bone, as viewed in Frankfurt horizontal
^4	**Nasion**		Midline of the fronto-nasal suture
^*5	**Rhinion**		Most anterior midline point at the inferior free end of the internasal suture
6	**Nasopinale**		Inferiormost midline point of piriform aperture
7	**Prosthion**		Anteroinferior point on projection of the premaxilla between the central incisors
8	**Prosthion2**	Right	Anteroinferiormost point on premaxilla equivalent to prosthion but between central and lateral incisors
9	Zygo-max inferior	Right	Anteroinferior point of zygomaticomaxillary suture, in anterolateral view
10	Zygo-max superior	Right	Anterosuperior point of zygomaticomaxillary suture, taken at orbital rim
^11	**Dacryon**	Right	Junction of the frontal, lacrimal, and maxilla
^12	Mid-torus inferior	Right	Point on inferior margin of supraorbital torus (superior margin of orbit) roughly at middle of orbit
^13	Mid-torus superior	Right	Superior to MTI on superior most point of supraorbital torus when viewed in Frankfurt horizontal
^14	**Frontomalare orbitale**	Right	Where the frontozygomatic suture crosses the inner orbital rim
^15	Frontomalare temporale	Right	Where the frontozygomatic suture crosses the lateral edge of the zygoma
^16	Porion	Right	Uppermost point on the margin of the external auditory meatus, in Frankfurt horizontal
^*17	***Zygo-temp superior***	Right	Superior point of zygomatico-temporal suture on lateral face of zygomatic arch
18	**Prosthion2**	Left	Anteroinferiormost point on premaxilla equivalent to prosthion but between central and lateral incisors
19	Zygo-max inferior	Left	Anteroinferior point of zygomaticomaxially suture, in anterolateral view
20	**Zygo-max superior**	Left	Anterosuperior point of zygomaticomaxillary suture, taken at orbital rim
^21	**Dacryon**	Left	Junction of the frontal, lacrimal, and maxilla
^22	Mid-torus inferior	Left	Point on inferior margin of supraorbital torus (superior margin of orbit) roughly at middle of orbit
^23	Mid-torus superior	Left	Superior to MTI on superior most point of supraorbital torus when viewed in Frankfurt horizontal
^24	**Frontomalare orbitale**	Left	Where the frontozygomatic suture crosses the inner orbital rim
^25	Frontomalare temporale	Left	Where the frontozygomatic suture crosses the lateral edge of the zygoma
^26	Porion	Left	Uppermost point on the margin of the external auditory meatus, in Frankfurt horizontal
^*27	***Zygo-temp superior***	Left	Superior point of zygomatico-temporal suture on lateral face of zygomatic arch
^28	Opisthion		Midline point at the posterior margin of the foramen magnum
^29	Basion		Midline point on the anterior margin of the foramen magnum
30	Hormion		Most posterior midline point on the vomer
31	Staphylion		Midline point on the palate on a line drawn tangent to the anterior most points on the choanae
32	**Incisivion**		Midline point at the posterior end of the incisive foramen
^33	*Postglenoid*	Right	Tip (or midpoint of area)
^*34	***Zygo-temp inferior***	Right	Inferolateral point of zygomaticotemporal suture on lateral face of zygomatic arch
^35	Distal M3	Right	Distal midpoint projected (laterally) onto alveolar margin
36	M1-2 contact	Right	Projected (laterally) onto alveolar margin
37	Mesial P3	Right	Most mesial point on P3 alveolus, projected on alveolar margin
38	**Premax-max-inferior**	Right	Anterior to canine
^39	Postglenoid	Left	Tip (or midpoint of area)
^*40	***Zygo-temp inferior***	Left	Inferolateral point of zygomaticotemporal suture on lateral face of zygomatic arch
^41	Distal M3	Left	Distal midpoint projected (laterally) onto alveolar margin
42	M1-2 contact	Left	Projected (laterally) onto alveolar margin
43	Mesial P3	Left	Most mesial point on P3 alveolus, projected on alveolar margin
44	**Premax-max-inferior**	Left	Anterior to canine

^ = missing from *Xenothrix*, **bold** = missing from *Paralouatta*, * = missing from MHD 20, underline = missing from PN-09-01, *italics* = missing from *Cartelles*.
[a] From Frost et al. (2003).

the inferior portions of the nasal bones are broken away. There are also holes in the left parietal, right lateral orbital rim, and right auditory bulla. All of the cranial sutures are closed and in various stages of fusion.

P^3-M^2 are fully erupted with wear evident at the cusp tips. Dental dimensions and morphology are consistent with other previously published descriptions of *Antillothrix* (e.g., Rímoli, 1977; Rosenberger et al., 2011) (Table 2). As with other specimens of *Antillothrix*, the anterior dentition is unfortunately lacking. However, all alveoli are present and mostly complete. Premolars are buccolingually wide with a pronounced protocone and slightly smaller paracone. P^4 has a more pronounced cingulum than P^3, which is most developed mesially in P^4, giving the tooth an overall "bean-shaped" appearance. M^1 is as buccolingually wide as P^4 with a clear trigon. The paracone and metacone are set somewhat lingually, giving the buccal aspect of the tooth a bulbous look. The hypocone arises from a prominent cingulum and is separated from the metacone by a distal fovea. The lingual cingulum continues around the tooth and tapers off on the mesial aspect of the protocone. As with other specimens of M^1 attributed to *Antillothrix*, a "distal crest" (MacPhee et al., 1995) runs between the protocone and the hypocone. Like M^1, M^2 has a prominent trigon, but overall the tooth is smaller. M^2 has a less well-developed buccal wall at the position of the metacone making M^2 much wider mesially than distally. The hypocone is very small and arises out of the cingulum. M^3 is missing from MHD 20, as in all other specimens of *Antillothrix*. However, the alveoli are present and indicate a mesiodistally compressed tooth that is approximately as buccolingually wide as M^2.

Despite being recovered in two separate caves, morphology shared between the two specimens makes it likely that MHD 20 and the previously published MHD 01 represent different ontogenetic growth stages of the same taxon (Fig. 4). Dental morphology is consistent across the two specimens. The dentition of MHD 01 includes large upper canine alveoli, which could indicate a male individual or pitheciine affinities (Rosenberger et al., 2011). The canine alveoli of MHD 20 are similar in absolute size to those of MHD 01 but with less influence from the roots on the convexity of the maxilla (Fig. 4; Table 2).

In terms of cranial morphology, particularly striking are the similarities in the shape of the dorsoventrally elongated orbital apertures and the superciliary bosses on either side of a deep depression at glabella, a combination of features sometimes seen in *Pithecia* and *Cebus* (Fig. 4; SOM Fig. S2). MHD 01 was initially

Table 5
Species mean cranial centroid size and species mean body mass values used to create the predictive body mass equations for MHD 20 (left) and PN-09-01 (right).

Specimen/Taxon	Centroid Size	Body Mass (g)[a]
MHD 20	179.51	OLS: 3231, PGLS: 3249
PN-09-01	162.01	OLS: 2583, PGLS: 2718
Alouatta belzebul	240.69/234.67	6395
Alouatta caraya	228.95/223.46	5383
Alouatta guariba	221.58/216.07	5175
Alouatta palliata	216.83/210.73	6250
Alouatta pigra	238.37/232.20	8915
Alouatta seniculus	238.06/232.27	5950
Ateles belzebuth	218.24/210.88	8167
Ateles fusciceps	223.08/215.25	9025
Ateles geoffroyi	208.39/201.17	7535
Ateles paniscus	219.71/211.98	8280
Brachyteles arachnoides	227.55/220.07	8840
Cacajao calvus	186.62/181.47	3165
Callicebus caligatus	127.28/122.55	880
Cebus albifrons	175.79/169.05	2735
Cebus apella	184.45/177.84	2936
Cebus capucinus	189.59/182.80	2861
Chiropotes satanas	167.02/158.90	2740
Lagothrix lagotricha	209.18/202.02	7150
Pithecia monachus	161.46/156.25	2360
Pithecia pithecia	152.66/147.42	1760

[a] Extant body mass taken from Isler et al. (2008).

described by Rosenberger et al. (2011) as similar to an extant *Cebus* due to its short face, close-set eyes, large smoothly vaulted braincase, flat glenoid fossa, and short postglenoid process. These features are elongated, widened, and overall more strongly developed in the fully adult specimen, which also has relatively strong temporal lines that are very sharply raised in the frontal trigon region. Based on the adult morphology now known to be exhibited by MHD 20, as well as evidence from the mandible (Rosenberger et al., 2013), the features of MHD 01 listed above are more correctly interpreted as indicative of its ontogenetic age rather than phylogenetic affinity with cebines.

One feature that all three known *Antillothrix* crania share is the steeply angled nuchal plane with a rugose occipital surface (Fig. 4). Kay et al. (2011b) interpret this as indicating a functional, rather than phylogenetic, association with *Alouatta,* which exhibits an even more extreme version of this trait. Rosenberger et al. (2011) also point out, however, that it is likely a primitive platyrrhine feature as it is seen in other fossil crania such as *Dolichocebus gaimanensis* and *Tremacebus harringtoni* as well (see Kay et al., 2008). All of these taxa also share a small endocranial volume for their estimated body size, which is likely a primitive feature for all of the major clades (i.e., Sears et al., 2008; Hartwig et al., 2011; Aristide et al., 2016) and could be influencing the truncated morphology of the posterior neurocranium (Halenar and Tallman, 2013). The endocranial volume of MHD 01 was originally reported as 58 ml by Rosenberger et al. (2011); this appears to have been a typographical error and a conservative estimate of 38 ml for the partial neurocranium is now the preferred value. PN-09-01 has an endocranial volume of 41 ml (Allen et al., 2012) while the MHD 20 endocranial volume measured here equals 39 ml. Both of the adult values are in the range of a small *Alouatta* or large *Pithecia* in absolute terms; when body size estimates are taken into account (see below), the relative values are intermediate between those two extant taxa (Table 1; Fig. 7). Reconstructions of the endocast of PN-09-01 reveal other similarities to *Alouatta*, not only in its small size but also the shape of the relatively smooth surface (Allen et al., 2012).

Kay et al. (2011b) mention some of the differences between MHD 01 and PN-09-01 and attribute them to the developmental age difference between the two specimens. MHD 20 is a fully adult specimen so comparisons between it and PN-09-01 will be more informative taxonomically. As described by Kay et al. (2011b), PN-09-01 has a broad interorbital region, deep zygomatic arch, strong postglenoid process, vertically oriented nuchal plane, unflexed cranial base, and strong temporal lines, features all seen to similar degrees in MHD 20 (Figs. 3–4). But there are some shape differences between the two adult specimens that could be of some importance (and that are also reflected in the bgPCA results described below). For example, the neurocranium of PN-09-01 is shorter and more globular with a more vaulted frontal, while MHD 20 has a more elongated brain case and sloping frontal (Fig. 4). The deep depression at glabella seen in MHD 20, and MHD 01, is much less developed in PN-09-01 and does not create the same angled bosses on the superiomedial corners of the orbital apertures (Fig. 4). The temporal lines are strong in both specimens but are straighter and more parallel in MHD 20 and more sinusoidal in PN-09-01. In lateral view, MHD 20 has a more airorynchous face, especially in the premaxilla, and an overall less flexed cranial base, which could be influenced by its slightly smaller brain size compared to PN-09-01 (Fig. 4). PN-09-01 has a sharper nuchal crest, which arises from the surface of the neurocranium like a small shelf, and the flattened, expanded mastoid regions on either side face inferiorly, rather than more laterally as in MHD 20. MHD 20 has a straighter squamosal suture and shorter squamous portion of the temporal and a more angled lambdoidal suture, giving the occipital a more triangular shape (Fig. 4).

Other aspects of the cranial suture pattern should also be noted. Kay et al. (2011b) state that one of the “most surprising” features of the PN-09-01 cranium is the catarrhine-like arrangement of the bones at pterion, where the frontal and sphenoid bones are in contact rather than the zygomatic and parietal, which contact each other in most platyrrhines. This original interpretation has recently been corrected by an examination of the pterion region using μCT (Fulwood et al., 2016); PN-09-01 can be characterized as a “typical” platyrrhine with zygomatic-parietal contact on both sides of the cranium, although there is some asymmetry in the degree of contact. Asymmetry in the pterion suture pattern is rare amongst extant platyrrhines, but occurs more frequently in atelids than other taxa (Ashley-Montagu, 1933; Hershkovitz, 1977; Halenar, 2015). MHD 20 also has the “typical” platyrrhine zygomatic-parietal contact on both sides (as does MHD 01 on the left side where the bones are preserved) (Figs. 3–4).

When comparing MHD 20 with extant platyrrhines, the fossil cranium exhibits very few traits that have been traditionally used to define or diagnose any of the living clades (SOM Fig. S2). As has been discussed by Kay et al. (2011b) for PN-09-01, the narrow interorbital region, gracile zygomatic arches, encephalized brain, and flexed cranial base with an anteriorly placed foramen magnum seen in the Cebinae are absent in MHD 20 as well. MHD 20 does not fall in the “dwarfed” body size range of the Callitrichinae (or the larger end of the body size spectrum occupied by the Atelidae) nor does it lack an M^3 like the marmosets and tamarins. The cranium does not have the enlarged nocturnally adapted orbits of *Aotus*. While the canines themselves are missing, from the alveoli it is clear that MHD 20 did not have enlarged everted canines like the pitheciins. And while a depression at glabella is sometimes seen in *Pithecia*, despite being broken, it seems that the nasal aperture of MHD 20 did not have a straight, broad upper border, a consequence of the exceedingly inferiorly wide nasal bones in that genus and the closely related *Cacajao* and *Chiropotes*. MHD 20 does not have the ventrally deflected zygomatic arch that extends below the alveolar margin like *Callicebus*, but the two do share the lack of a diastema between the canines and lateral incisors, as well as upper canine alveoli whose buccolingual breadth is small relative to the breadth of the alveolus of P^4 (Table 2; see further discussion of the potential

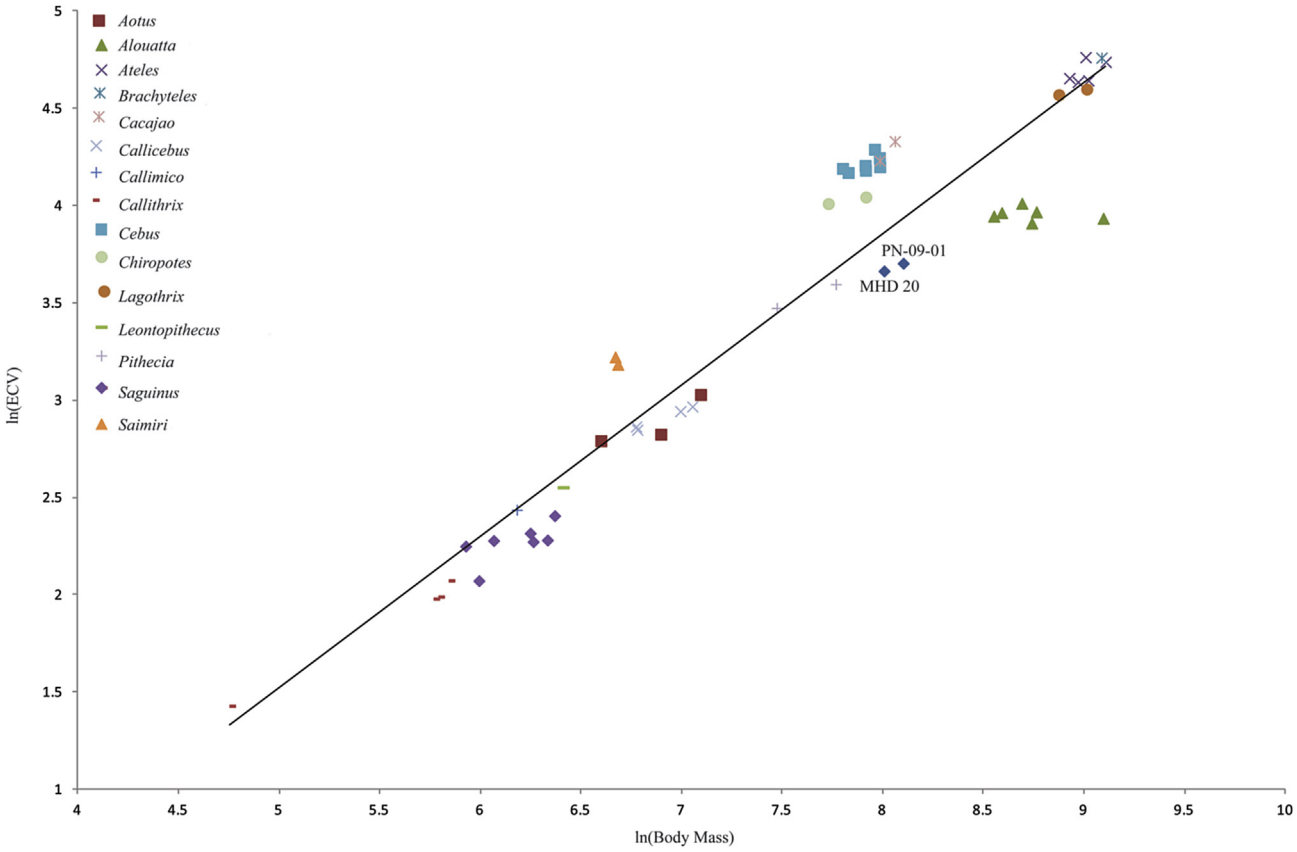

Figure 7. Platyrrhine data from Isler et al. (2008) Figure 4, re-plotted with the addition of the MHD 20 and PN-09-01 endocranial volumes and mean estimated body mass (PN-09-01 values from Allen et al., 2012). Note the position of both *Antillothrix* specimens below the regression line ($y = 0.78x-2.36$, $R^2 = 0.91$). (For interpretation of the references to color in this figure legend, the reader is referred to the web version of this article.)

cladistic importance of these traits below). While none of the following traits is as extreme in MHD 20 as it is in *Alouatta*, as mentioned above, the elongated cranial base, airorynchous face, small brain size relative to body size, and posteriorly facing nuchal plane and foramen magnum are reminiscent of the howler cranium.

4.2. 3DGM analyses

Several different between-group principal components analyses were run using different landmark sets to include fragmentary fossil specimens. As *Cartelles*, PN-09-01, and MHD 20 are nearly complete, the most conspicuously absent or incomplete features being the zygomatic arches, they preserve the most inclusive set of landmarks and were analyzed together, first with the extant sample. MHD 20 and *Cartelles* fall in a central, otherwise unoccupied region of the morphospace and are outside any of the convex hulls that define the shape variation exhibited by the extant platyrrhine genera, while PN-09-01 is within the *Lagothrix, Brachyteles,* and *Ateles* distributions (Fig. 8). MHD 20 and *Cartelles* are between *Alouatta* which lies toward the negative end of bgPC1 (which represents 73% of the variance between the group means and 68% of the variance between individuals) and the rest of the extant taxa which lie toward the positive end of bgPC1 (Fig. 8). MHD 20 is connected to PN-09-01 by the minimum spanning tree; PN-09-01 is in turn connected to the *Brachyteles* mean shape.

The small sample size for *Brachyteles* ($n = 4$) compared to many of the other taxa in the comparative sample should be noted here; if the sample were to be increased, it is possible the genus distribution would expand to fill some of the shape space between the atelins and *Alouatta* given its neurocranial shape similarities shared with the former and dietary adaptations shared with the latter. While this two-dimensional simplification of the variation makes it seem like PN-09-01 and MHD 20 are far away from one another in shape space, the Procrustes distance between the two specimens is 0.08; this is well within the range of pairwise Procrustes distances seen within the extant species ($d = 0.04–0.17$, mean = 0.07, standard deviation = 0.02) and extant genera ($d = 0.04–0.20$, mean = 0.09, standard deviation = 0.02; Fig. 9). Distances between individuals of different genera ranged from 0.05 to 0.42 (mean = 0.18, standard deviation = 0.06) with the highest values between individuals of *Alouatta* and the rest of the sample (Fig. 9). Also of note, the centroid size of the individual specimens is not the main driver of their distribution across bgPC1 ($R^2 = 0.50$ for a regression of the natural logarithm of centroid size against the bgPC1 scores), but the larger size of the *Cartelles* cranium compared to the other taxa in the analysis could be contributing to its position outside the convex hull of *Alouatta*, a taxon it has been both phenetically and phylogenetically linked to in previous studies (i.e., Hartwig and Cartelle, 1996; Halenar, 2012; Halenar and Rosenberger, 2013; Rosenberger et al., 2015b).

As shown by the wireframes in Figure 8, the main axis of shape variation on bgPC1 is being driven by differences in face size and palate shape, cranial base angle and the orientation of the foramen magnum, and bregma height, with *Alouatta* and *Cebus/Saimiri* on opposite ends of the axis. *Alouatta* has a large face and palate with narrow incisors and a long molar row, an obtuse cranial base angle and posteriorly oriented foramen magnum, and a flattened, poorly

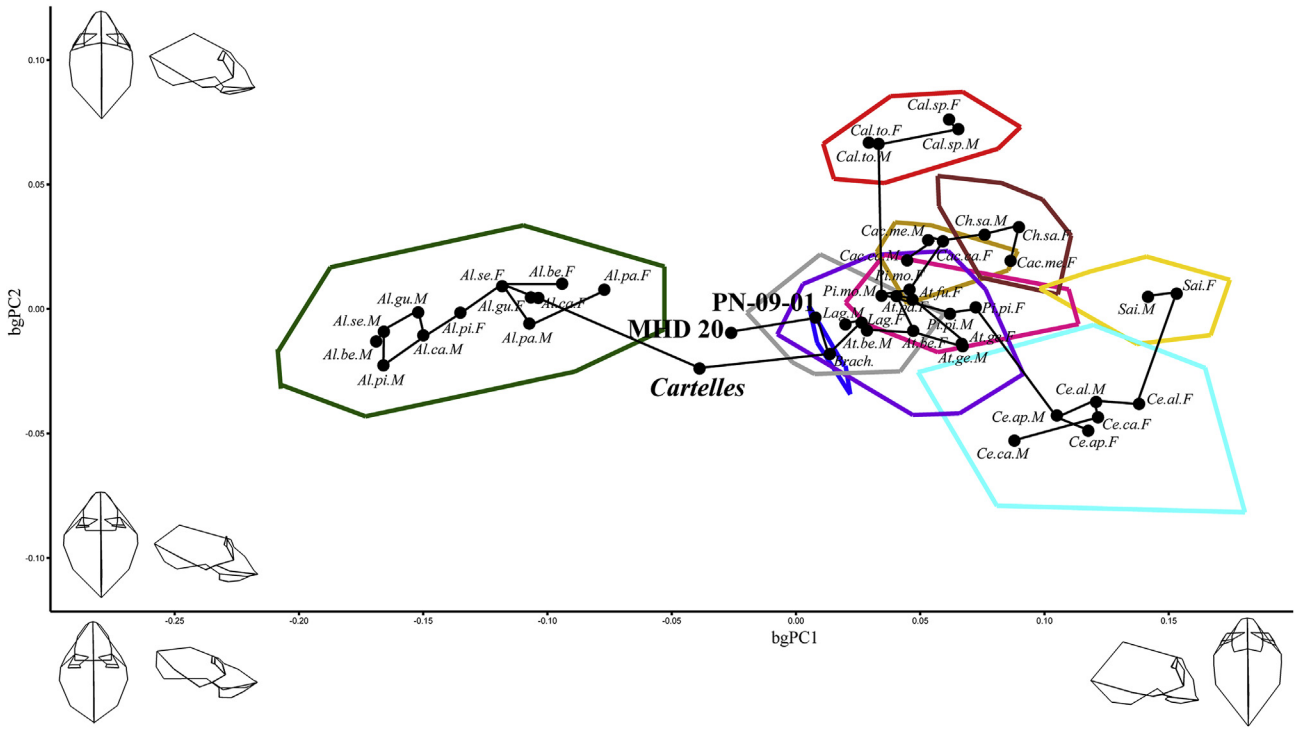

Figure 8. Plot of bgPC1 vs. bgPC2, from between-group principal components analyses including all extant specimens, MHD 20, PN-09-01, and *Cartelles*. Black dots represent male and female species mean shapes which are connected by a minimum spanning tree and surrounded by the convex hull defining the distribution of the individual specimens of each genus in the morphospace. Teal = *Cebus*, bright yellow = *Saimiri*, dark yellow = *Cacajao*, brown = *Chiropotes*, pink = *Pithecia*, red = *Callicebus*, purple = *Ateles*, gray = *Lagothrix*, blue = *Brachyteles*, green = *Alouatta*. Wireframes represent the shapes of the extant specimens at the extreme end of each axis in both lateral and inferior views. (For interpretation of the references to color in this figure legend, the reader is referred to the web version of this article.)

encephalized neurocranium, while *Cebus* and *Saimiri* have the opposite set of features. MHD 20 and *Cartelles* have less pronounced versions of these classic *Alouatta* features, hence their position towards that extant taxon on bgPC1. As discussed above, PN-09-01 has a shorter, more globular braincase and a shorter, less airorynchous face as compared to MHD 20 so it is not surprising that it falls farther away from the *Alouatta* distribution. On bgPC2 (7% of the variance between the group means and 6% of the variance between individuals), *Callicebus* individuals differ from the other species in having more positive scores due to their extreme zygomatic length and narrow cranium; other important aspects of shape change on this axis include bregma position in the anterior/posterior direction, orbital aperture size and shape, and parallel vs. parabolic premolar/molar rows.

The addition of *Paralouatta* to this analysis does not drastically affect the distribution of the sample across shape space, even though many midfacial landmarks must be excluded (Fig. 10). MHD 20 and *Cartelles* appear closer to the convex hull defining the *Alouatta* range of variation on the positive end of bgPC1 (representing 71% of the variance between the group means and 66% of the variance between individuals) (Fig. 10). MHD 20 is most similar to the *Alouatta belzebul* female mean shape and to PN-09-01 (which is still closest to the *Brachyteles* mean shape) while *Cartelles* is most similar to the *Lagothrix* male mean shape. *Paralouatta* falls within the *Alouatta* convex hull and is connected to the *Alouatta guariba* female mean shape by the minimum spanning tree. *Callicebus* and *Cebus* again occupy opposite ends of bgPC2 (8% of the variance between the group means and between individuals). The aspects of cranial shape driving the variation along each axis are similar to those described above with centroid size again only minimally affecting the distribution ($R^2 = 0.50$ for a regression of the natural logarithm of centroid size against the bgPC1 scores).

A third set of analyses were run including MHD 20, PN-09-01, *Cartelles*, and *Xenothrix*; *Paralouatta* was not included as many of the landmarks missing on the MNHN V194 cranium are the same few that are preserved on the AMNH 268006 partial face and palate (Table 4). The results of these analyses paint a slightly different picture for the fossils and suggest that it is the shape of the upper face and neurocranium that makes them look more distinct compared to the extant taxa in the analyses described above. bgPC1 (now representing 43% of the variance between the group means and 40% of the variance between individuals) distinguishes between the large-faced *Alouatta* toward the negative end and the small-faced *Cebus/Saimiri* toward the positive end ($R^2 = 0.60$ for a regression of ln centroid size on the individual specimen bgPC1 scores) (Fig. 11). Shape changes across bgPC1 are driven by the width of the premaxilla, the length and orientation of the zygomaticomaxillary suture (particularly the placement of the superior end where the suture crosses the orbital rim), and the position of hormion relative to staphylion, which is related to airorynchy of the face.

On bgPC2 (23% of the variance between the group means and 20% of the variance between individuals), *Callicebus* is again distinct from the rest of the taxa due to its elongated zygomatic bones and a dentition that is more evenly spaced around a more parabolic tooth row (Fig. 11). bgPC3 represents a larger portion of the variance than in previous analyses (13% of that between the group means and 10% between individuals); taxa with a wider incisor row and bicanine breadth and a square palate like *Ateles, Cacajao*, and *Cartelles* have more positive scores on this axis while taxa with narrower incisors but a wider distance between their molars like *Cebus* and *Callicebus* have more negative scores (Fig. 12).

All of the fossils now fall within the boundaries of the genus-defining convex hulls: MHD 20 and *Cartelles* are within the

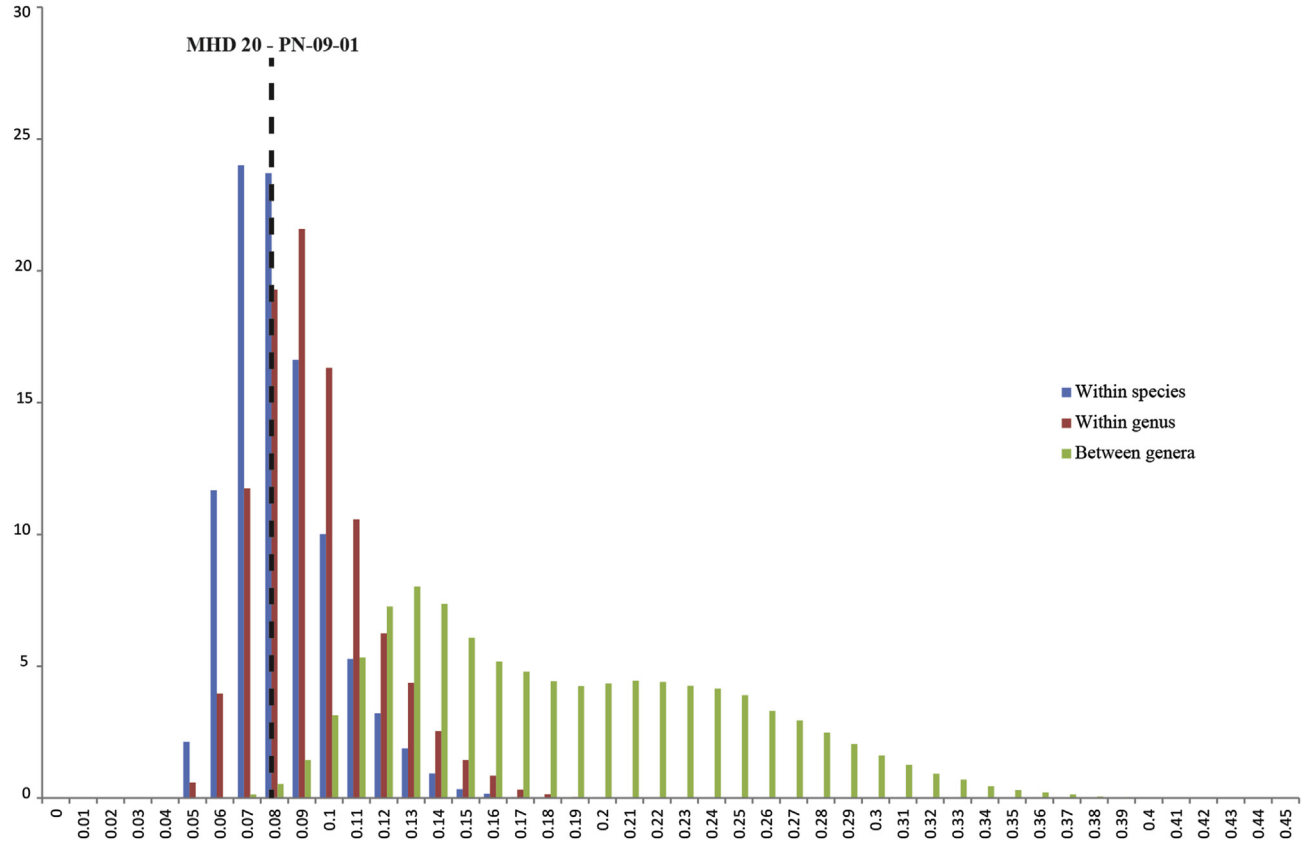

Figure 9. Distribution of pairwise Procrustes distances between individuals of the same species (blue), same genus (red), and different genera (green) in the extant sample when using the most complete landmark configuration. The Procrustes distance between MHD 20 and PN-09-01 (0.08) is shown by the dashed line and is very close to the average pairwise distance seen within both extant species and extant genera. (For interpretation of the references to color in this figure legend, the reader is referred to the web version of this article.)

Alouatta distribution, PN-09-01 falls within the intersection of the shape space occupied by *Alouatta* and *Ateles*, and *Xenothrix* is within the intersection of *Cebus, Cacajao,* and *Pithecia* (Fig. 11). MHD 20 is linked by the minimum spanning tree to the mean female *A. belzebul* face/palate shape, *Cartelles* to the *Alouatta seniculus* male, PN-09-01 to the *Brachyteles* mean shape (although it falls outside the shape space occupied by the four *Brachyteles* specimens on the first three bgPC axes), and *Xenothrix* to the *Cacajao calvus* female (Figs. 11–12). While they are no longer linked together by the minimum spanning tree, the lower face and palate of MHD 20 and PN-09-01 are still relatively close together in shape space; the Procrustes distance between the two specimens is 0.11 which is well within the range of pairwise Procrustes distances within a single species (d = 0.04–0.18, mean = 0.09, standard deviation = 0.02) and within a genus (d = 0.05–0.21, mean = 0.10, standard deviation = 0.02) seen in the extant taxa (Fig. 13).

The position of *Xenothrix* is an unexpected result, as the lack of a diastema between its reduced canine and lateral incisors and relatively long zygomatic bones have been used to ally the genus with *Callicebus* by previous authors (e.g., MacPhee and Horovitz, 2004). The fossil is linked with *Cacajao* here based on their similar palate widths and less extreme zygomatic positioning compared to *Callicebus*, despite differing in features like canine size and orientation. While *Xenothrix* was not the target of this investigation, and this is a phenetic rather than phylogenetic analysis, these results suggest that further morphometric and comparative anatomical work could benefit our phylogenetic understanding by focusing on the overall shape of the *Xenothrix* face/palate rather than relying only on a few discrete characters pertinent to cladistic analysis. Furthermore, with the differing results seen here for *Cartelles* and MHD 20 when landmarks covering the whole cranium or just the lower face were included, it is possible that the overall phenetic relationships of *Xenothrix* would change if more complete cranial specimens are recovered.

In summary, the shape of the MHD 20 cranium is intermediate between that of *Alouatta* and the atelines as a consequence of its large and relatively airorynchous face and parabolic dental arcade combined with its uniquely shaped upper face, which includes a depressed glabella and raised superciliary bosses, and slightly narrow and elongated neurocranium with a rugose, flattened, and laterally expanded nuchal plane. The palate and lower face are the parts of the fossil crania that are most similar to the shape of the extant taxa. *Cartelles* and MHD 20 both have relatively large, airorynchous faces with a wide premaxilla, similar to the overall facial profile seen in *Alouatta*. *Xenothrix* and *Callicebus* have a similarly shaped palate and share a lack of a diastema between the canine and lateral incisor, but the extremely elongated zygomatic bones of *Callicebus* make its face distinct from all of the other taxa. While MHD 20 and PN-09-01 appear at first glance to fall relatively far from one another in shape space, the Procrustes distance between them is within the range of pairwise Procrustes distances seen between two individuals of the same species and of the same genus in the extant sample. There is no reason to conclude from the 3DGM analyses presented here that they do not both belong to *A. bernensis* despite some of the morphological differences between them described above. Whether these results have phylogenetic implications for any of the fossils involved is yet to be determined.

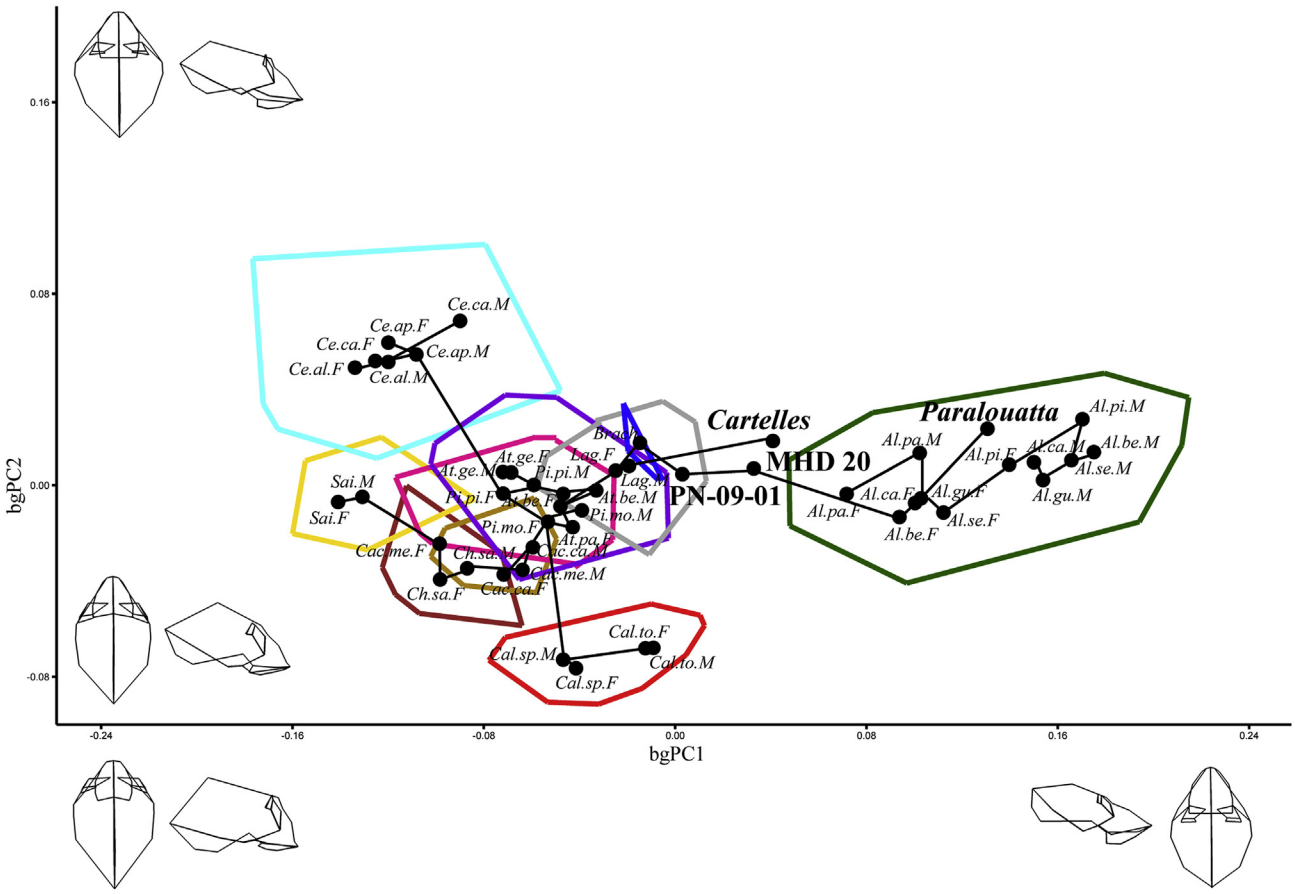

Figure 10. Plot of bgPC1 vs. bgPC2, from between-group principal components analyses including all extant specimens, MHD 20, PN-09-01, *Cartelles*, and *Paralouatta*. Black dots represent male and female species mean shapes which are connected by a minimum spanning tree and surrounded by the convex hull defining the distribution of the individual specimens of each genus in the morphospace. Teal = *Cebus*, bright yellow = *Saimiri*, dark yellow = *Cacajao*, brown = *Chiropotes*, pink = *Pithecia*, red = *Callicebus*, purple = *Ateles*, gray = *Lagothrix*, blue = *Brachyteles*, green = *Alouatta*. Wireframes represent the shapes of the extant specimens at the extreme end of each axis in both lateral and inferior views. (For interpretation of the references to color in this figure legend, the reader is referred to the web version of this article.)

4.3. Body size

The juvenile *Antillothrix* MHD 01 was estimated to weigh approximately 4.2–5.6 kg based on M_1 regressions from its mandibular remains (Rosenberger et al., 2011). This is similar to the 4.5–5.0 kg estimate given by MacPhee and Meldrum (2006) for the UF 28038 mandible. All authors note, however, that these could be overestimates as the specimens appear to have relatively large teeth; the mandibular centroid size of MHD 01, for example, is similar to that of *Pithecia* (Rosenberger et al., 2011), which ranges in body weight from 1.6 to 2.6 kg (Isler et al., 2008). A similar situation arises when using estimates from the centroid size of various postcranial joint surfaces, where estimates average 4.4 kg for *Antillothrix* as a genus (Perry et al., 2015). The long bones of *Antillothrix* appear to be relatively robust (Rosenberger et al., 2011), again potentially resulting in an overestimate of body size. The centroid size of the MHD 20 cranium is, like the mandible, also slightly larger than that of *Pithecia* (Table 5). The newly developed predictive equation based on the OLS regression of extant species mean cranial centroid size and species mean body mass from Isler et al. (2008) ($y = 3.5011x-10.119$ with an R^2 of 0.87, SEE = 0.237, %SEE = 26.724, QMLE = 1.028) gives an estimate for MHD 20 of approximately 3.2 kg (Table 5). The PGLS regression ($y = 2.701x-2.606$ with an R^2 of 0.73, SEE = 0.370, % SEE = 44.676, QMLE = 1.0) returned a very similar estimate (Table 5).

This estimate is only slightly smaller than the average of 3.3 kg obtained for PN-09-01 based on a set of craniodental dimensions (Allen et al., 2012). But again, this could be an overestimate for that specimen as it is also based partly on dental measures. The PN-09-01 cranium is slightly smaller than MHD 20 in most linear dimensions (Table 1) and therefore that individual might be expected to have a slightly smaller body mass. A second equation was developed here for PN-09-01 using the cranial centroid size method; this was necessary as this specimen is missing several landmarks that are preserved on MHD 20 (see Table 4). These extra missing landmarks are also why the PN-09-01 centroid size is quite a bit smaller, at 162.01 (Table 5), despite the crania themselves having more similar linear dimensions (Table 1). The OLS regression equation ($y = 3.4026x-9.485$, $R^2 = 0.86$, SEE = 0.248, % SEE = 28.120, QMLE = 1.031) returns a body size estimate for PN-09-01 of 2.6 kg while the PGLS-based estimate was 2.7 kg ($y = 2.636x-2.421$, $R^2 = 0.72$, SEE = 0.377, %SEE = 45.736, QMLE = 1.073) (Table 5).

5. Discussion

5.1. Can MHD 20 provide new information about the paleobiology of Antillothrix?

While cranial remains are typically not used to reconstruct the locomotor behavior of fossil taxa, there is some information to be

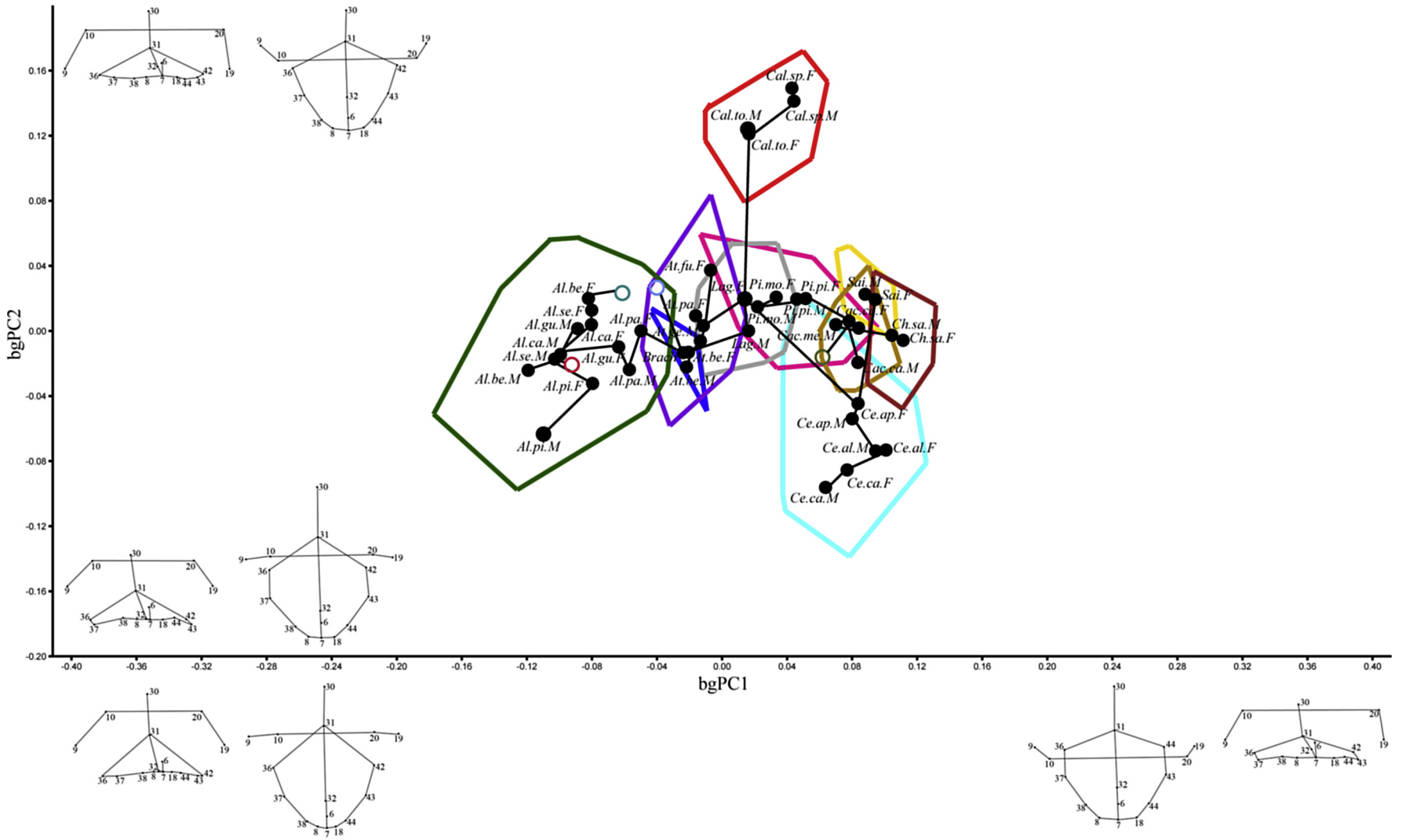

Figure 11. Plot of bgPC1 vs. bgPC2, from a between-group principal components analysis including all extant specimens, MHD 20, PN-09-01, *Cartelles*, and *Xenothrix*. Black dots represent male and female species mean shapes which are connected by a minimum spanning tree and surrounded by the convex hull defining the distribution of the individual specimens of each genus in the morphospace. Open circles are the fossils (Red = *Cartelles*, Green = MHD 20, Blue = PN-09-01, and Olive = *Xenothrix*). Teal = *Cebus*, bright yellow = *Saimiri*, dark yellow = *Cacajao*, brown = *Chiropotes*, pink = *Pithecia*, red = *Callicebus*, purple = *Ateles*, gray = *Lagothrix*, blue = *Brachyteles*, green = *Alouatta*. Wireframes represent the shapes of the extant specimens at the extreme end of each axis in both anteroblique and superior views; numbers correspond to the landmarks defined in Table 4 that are preserved on the *Xenothrix* specimen. (For interpretation of the references to color in this figure legend, the reader is referred to the web version of this article.)

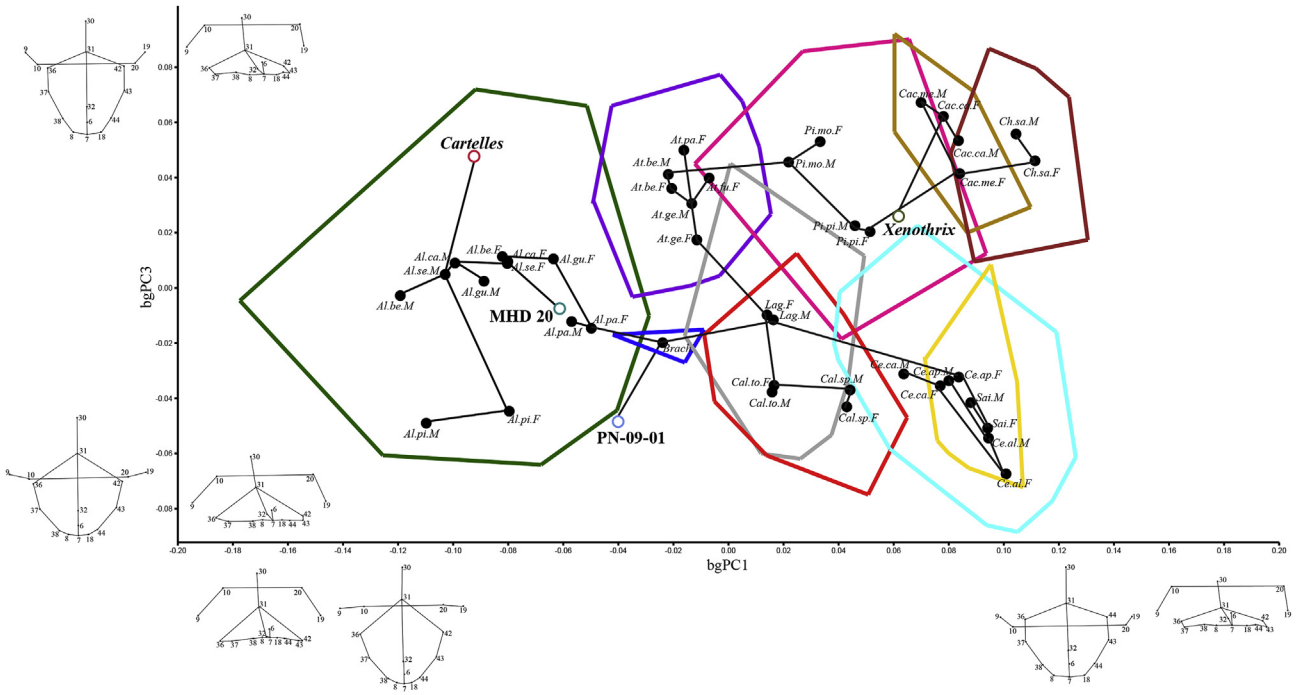

Figure 12. Plot of bgPC1 vs. bgPC3, from a between-group principal components analysis including all extant specimens, MHD 20, PN-09-01, *Cartelles*, and *Xenothrix*. Black dots represent male and female species mean shapes which are connected by a minimum spanning tree and surrounded by the convex hull defining the distribution of the individual specimens of each genus in the morphospace. Open circles are the fossils. Teal = *Cebus*, bright yellow = *Saimiri*, dark yellow = *Cacajao*, brown = *Chiropotes*, pink = *Pithecia*, red = *Callicebus*, purple = *Ateles*, gray = *Lagothrix*, blue = *Brachyteles*, green = *Alouatta*. Wireframes represent the shapes of the extant specimens at the extreme end of each axis in both anteroblique and superior views; numbers correspond to the landmarks defined in Table 4 that are preserved on the *Xenothrix* specimen. (For interpretation of the references to color in this figure legend, the reader is referred to the web version of this article.)

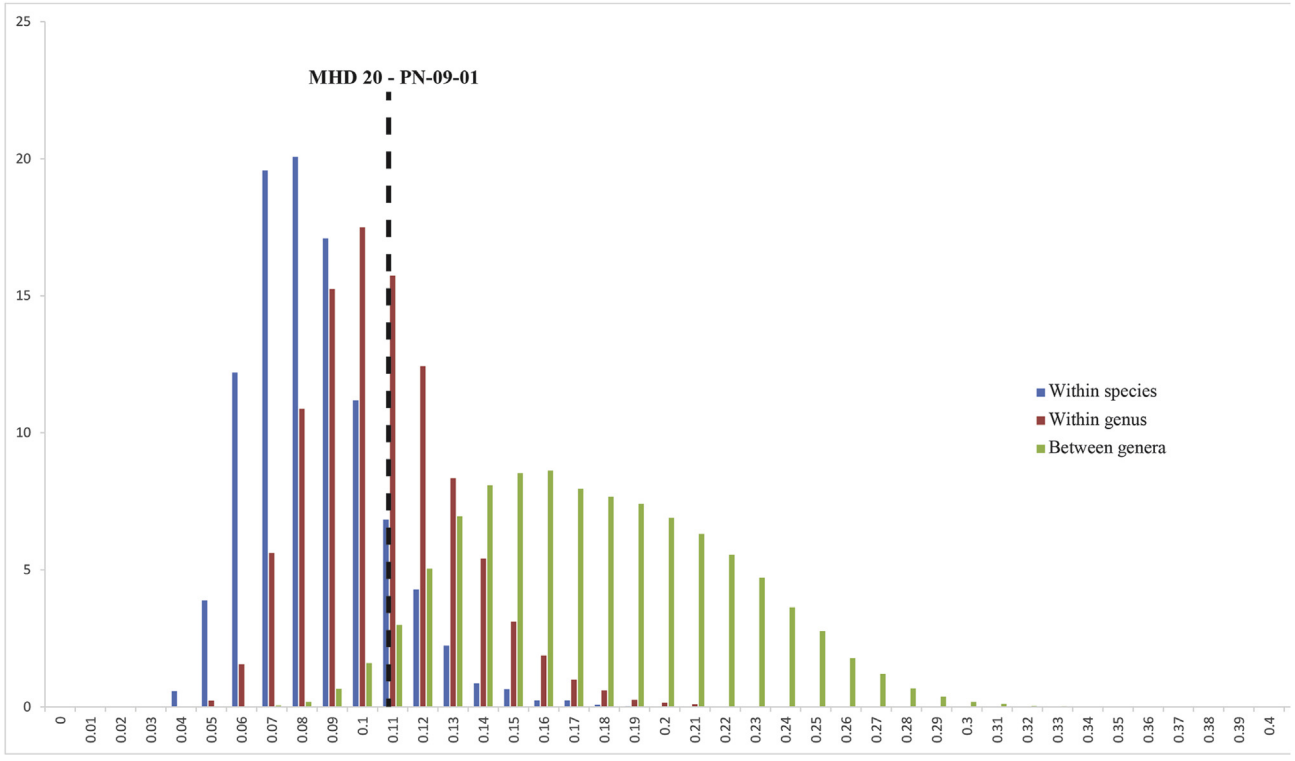

Figure 13. Distribution of pairwise Procrustes distances between individuals of the same species (blue), same genus (red), and different genera (green) in the extant sample when using the landmark configuration describing only the face/palate as preserved in *Xenothrix* (AMNH 268006). The Procrustes distance between MHD 20 and PN-09-01 (0.11) is shown by the dashed line and is well within the range seen for both extant species and extant genera. (For interpretation of the references to color in this figure legend, the reader is referred to the web version of this article.)

gained regarding head carriage and body postures. For example, the rugose posteriorly directed nuchal region of PN-09-01, which is also seen in MHD 20 and is similar to the condition seen in *Alouatta*, has been interpreted as evidence that *Antillothrix* included a comparably large percentage of tail and hindlimb suspension in its locomotor repertoire (Kay et al., 2011b). The robust joint surfaces suggested by the body size estimates discussed above, however, would seem to contradict suspension as a main locomotor mode in favor of a higher percentage of arboreal quadrupedalism and/or climbing. This is also supported by recent morphometric analyses of various tibiae (Rosenberger et al., 2015a) and remains from the pelvic and pectoral girdles (Gladman and Rosenberger, 2013) that have been attributed to *Antillothrix*. Two proximal femora also found in the Padre Nuestro cave and attributed to *Antillothrix*, however, have been classified by discriminant function analysis as functionally similar to *Aotus* and *Saimiri*, taxa that practice a fair amount of leaping (Cooke and Tallman, 2012); similar results were obtained for a distal humerus, which was classified as *Chiropotes*-like, although with less robust support (Tallman and Cooke, 2016).

Dental remains of *Antillothrix* have historically been better represented in the fossil record and therefore robust dietary reconstructions already exist for this taxon. The teeth of MHD 20 are morphologically similar to all other known specimens and offer no contradictory information to previous studies. Dietarily, *Antillothrix* was likely a mixed feeder, potentially consuming leaves and fruit (Cooke, 2011), though based on microwear analyses of lower molars, Kay and colleagues have suggested that hard objects may have played an important role in its diet (Kay et al., 2011a). Its lower molar morphology shows similar levels of dental relief and shearing potential as *Callicebus*, *Aotus*, and the extinct Patagonian genera *Dolichocebus* and *Carlocebus* (Cooke, 2011). Given its geographic location at the northern extreme of the platyrrhine radiation, this taxon may have been living in marginal environments with some degree of seasonality, thus making dietary flexibility essential. Today, the region where *Antillothrix* once lived is covered with dry scrub forest. Based on lake core sediment from Lake Miragoane in southwestern Haiti, Higuera-Gundy et al. (1999) have suggested a cool and dry environment in Hispaniola during the early Holocene, but there are few data available regarding Hispaniolan paleoecology and paleoclimate before 10,000 years ago, making interpretations about the environment in which *Antillothrix* first evolved – evidence indicates the species was alive during the Pleistocene (Rosenberger et al., 2015a) – difficult.

At approximately 3–4 kg, *Antillothix* occupies a body size niche not frequently seen in extant mainland platyrrhines so it is hard to use a similarly-sized taxon as an analog for behavior. *Antillothrix* is slightly larger than an average *Cebus* or pithecid and several kilograms smaller than the atelids (Isler et al., 2008). This body size window, however, is also occupied by the other Caribbean primates (except for *Paralouatta* which is more similar to the mainland atelids at approximately 7–9 kg; MacPhee and Meldrum, 2006; Perry et al., 2015) suggesting that there may have been aspects of their island habitats that selected for a narrower range of body sizes overall compared to those on the mainland.

5.2. Can MHD 20 help us evaluate the phylogenetic relationships of Antillothrix?

Our detailed phenetic analysis should be seen as a complement to the phylogenetically oriented studies produced by a number of researchers. Multiple hypotheses of relationships have been proposed for the Greater Antillean primates in relation to each other as well as to extant mainland taxa. The main ideas are shown schematically in Figure 14. Originally, as each new fossil was discovered, it was suggested to be closely related to a specific clade on the mainland. *Paralouatta*, as its name implies, was argued to be an alouattine (Rivero and Arredondo, 1991). Similarly, *Antillothrix* was first named as an extinct species of the living squirrel monkey, *Saimiri* (Rímoli, 1977), though Ford suggested a callitrichine affinity based on tibial morphology (Ford and Morgan, 1986). *Xenothrix* has been allied with *Callicebus* (Rosenberger, 1977; Horovitz, 1997; MacPhee and Horovitz, 2004) and *Aotus* (Rosenberger, 2002). Based mostly on dental characters, all three of the Caribbean genera were suggested to be part of a monophyletic pitheciid group, most closely related to *Callicebus* (MacPhee et al., 1995; Horovitz and MacPhee, 1999; MacPhee and Horovitz, 2004). Most recently, Kay (2015) has proposed that the Caribbean forms are stem platyrrhines, which do not form a monophyletic group.

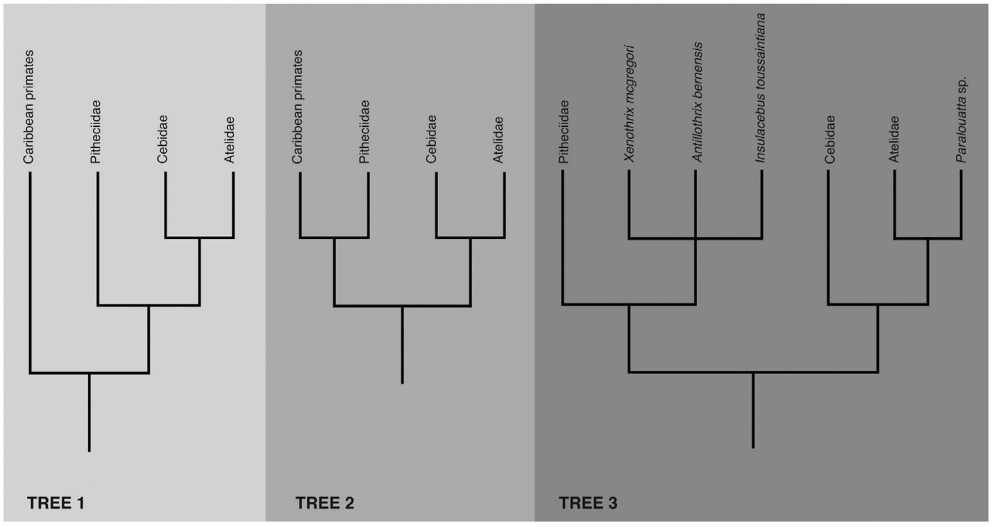

Figure 14. Schematic cladograms showing hypothesized relationships of the Caribbean platyrrhines. Branching patterns of the three platyrrhine families after Perelman et al. (2011). Tree 1 shows the Caribbean platyrrhines as a stem group or groups that are not necessarily monophyletic and fall outside the clade of extant platyrrhine families (e.g., Kay, 2015). Tree 2 shows the Caribbean platyrrhines as a monophyletic group within Pitheciidae (e.g., MacPhee et al., 1995; Horovitz and MacPhee, 1999; MacPhee and Horovitz, 2004); MacPhee and colleagues have further advocated for a sister-group relationships with *Callicebus*, not shown here. Tree 3 shows one version of the multi-origin scheme with *Paralouatta* species as atelids, most closely related to extant *Alouatta,* and the other Caribbean forms as pitheciids (e.g., Rosenberger et al., 2011, 2013, 2015b).

Several of the most informative characters in the matrix of Horovitz and MacPhee (1999) and MacPhee and Horovitz (2004) can now be evaluated in better detail with the addition of the PN-09-01 and MHD 20 cranial specimens (Table 6). The one cranial (i.e., non-dental) character linking all of the Antillean taxa together as a monophyletic clade in those previous analyses was a nasal fossa that overhangs the boundaries of the palate, though it was not possible to code this character in *Antillothrix* at the time. Kay et al. (2011b) say that this character state is not present in PN-09-01, and note instead that it has a "typical" platyrrhine narrow nasal fossa. This is confirmed here from the CT scan of PN-09-01 and also seems to be the case in MHD 20 (Fig. 15).

A word of caution should be inserted here, however, about the homologous nature of this feature across these fossil taxa. The character was originally defined as a nasal fossa that is wider than the palate at the level of M^1 (Horovitz, 1997). In their description of the *Xenothrix* face (AMNH 268006), MacPhee and Horovitz (2004) also characterize the condition as a nasal fossa that is "wider than the palate at the latter's widest point" (p.1). The widest point of the palate is at the level of M^1 in *Xenothrix*, but is more posterior, at the level of M^2, in *Antillothrix* and even more posterior, closer to M^3 (which is now anterior to the choanae), in *Paralouatta* (SOM Fig. S3). It is therefore hard to ensure that this character is being observed at a homologous position on each fossil as their faces are quite different in terms of relative size, airorynchy, number of molars, and shape of the palate. The more posterior position on MHD 20 and PN-09-01 allows for the use of the maxillo-palatine suture as a clear standardized boundary for the palate when judging the relative widths of these structures. Wherever it is being observed it seems clear, with the addition of the new *Antillothrix* cranial material as a comparison, that *Xenothrix* is different from the other Antillean taxa, not in having a particularly wide nasal fossa but in having a more narrow palate (see also its unique v-shaped maxillo-palatine suture; Fig. 15, SOM Fig. S3).

One of the cranial characters that links the Antillean taxa specifically with extant *Callicebus* in the Horovitz and MacPhee (1999, 2004) analyses is the position of the root of the zygomatic arch, which extends below the alveolar border of the molars in extant titi monkeys (Table 6). The preserved portions of the zygomatic roots suggest that they do not extend below the alveolar border in MHD 20, or any of the other *Antillothrix* specimens (Figs. 3–4). While MacPhee and Horovitz's (2004) Figure 9E makes it seem like this is also the case for *Xenothrix*, the results of the principal components analysis described above do not indicate that *Xenothrix* shares this trait with *Callicebus.* Instead, it shows the fossil with a less extreme version of zygomatic lengthening more similar to that seen in the pitheciins. Nor is this feature present in *Paralouatta* – while the character is coded as missing in their character matrix, in the qualitative description of the *Paralouatta* cranium Horovitz and MacPhee (1999) state that "the preserved part of its ventral edge lies just above the plane of the alveolar border" (p. 39). Given that the zygomatic roots cannot be unequivocally shown to extend below the alveolar border in any of the Caribbean fossils, recently discovered or not, this trait is of questionable importance as evidence for a phylogenetic linkage with extant *Callicebus*.

The other cranial character cited by Horovitz and MacPhee (1999) as derived for *Callicebus* and the Caribbean taxa is the presence in the middle ear of paired prominences on the cochlear housing (Table 6). The interpretation of this feature as a derived trait is offered despite this character state being widely distributed among platyrrhines; it was coded as present in *Callicebus*, *Saimiri, Pithecia, Cebus, Aotus*, and in the callitrichines. Also, at the time of the original analysis, the only fossil cranium from the Caribbean to preserve this morphological region was that of *Paralouatta*. Kay et al. (2011b) state that the PN-09-01 *Antillothrix* cranium exhibits only one cochlear coil bulging into the middle ear. Compared to illustrations in Hershkovitz (1977), MHD 20 appears most similar to extant examples that exhibit paired prominences, but with no graphic definition of the alternative character states as defined by Horovitz and MacPhee (1999) it is hard to know how to make use of this trait in current comparative analyses of the fossils.

One synapomorphy shared between the Caribbean taxa and *Callicebus* suggested by the Horovitz and MacPhee analyses (i.e., Horovitz and MacPhee, 1999; MacPhee and Horovitz, 2004) that is supported by the new information from MHD 20 is a maxillary canine alveolus whose buccolingual breadth is smaller than that of the alveolus for P^4 (Table 6). In both the Horovitz and MacPhee (1999) and MacPhee and Horovitz (2004) matrices, this character was coded as primitive (i.e., large) for *Antillothrix* and derived (i.e., small) for *Callicebus, Paralouatta*, and *Xenothrix*. The MNHN V194 *Paralouatta* cranium is broken and does not preserve a complete canine alveolus to compare to its P^4 so should perhaps more conservatively be coded as "missing". The type specimen of *Antillothrix* (CENDIA-1), though abraded, was re-measured by L.B.H. and actually has a canine alveolus that is smaller buccolingually than the P^4 alveolus (Table 2a). Kay et al. (2011b) suggest that the PN-09-01 cranium has relatively large canines, although no measurements are given; L.B.H. measured the relevant dental dimensions in Geomagic Studio 2014 on a reconstructed surface from a CT scan of PN-09-01 and found that it too has a canine alveolus smaller than its P^4. The MHD 20 upper canine alveoli are relatively well-preserved and its P^4s are present; in this *Antillothrix* specimen, the canine alveolus is also smaller than that of the fourth premolar to a degree similar to that found in *Callicebus* and *Xenothrix* (Table 2a).

It should also be noted that this feature is likely tied to sexual dimorphism as well as dietary adaptation. For example, the

Table 6
Characters that were suggested by Horovitz and MacPhee (1999) and MacPhee and Horovitz (2004) to link the Caribbean taxa phylogenetically to *Callicebus* and the Caribbean taxa with each other as a monophyletic group, many of which were previously unknown in *Antillothrix*.

	Callicebus	*Xenothrix*	*Paralouatta*	*Antillothrix*	PN-09-01	MHD 20
Caribbean + *Callicebus*						
1. Middle ear, paired prominences on cochlear housing; 0 = absent, 1 = present	1	?	1	?	0	1
2. Zygomatic arch, ventral extent; 0 = below plane of alveolar border of posterior cheek teeth, 1 = above plane of alveolar border	0	0 (1)[a]	? (1)	?	1	1
3. C^1 alveolus size relative to P^4 equivalent; 0 = C^1 larger than P^4, 1 = C^1 smaller or equal to P^4	1	1	1 (?)	0 (1)	1	1
Caribbean Monophyly						
4. Nasal fossa width; 0 = narrower than palate at level of M^1, 1 = wider	0	1	1	?	0	0

[a] Coding not in parentheses is from the original matrices. See the main text for explanations of equivocal character states listed here in parentheses.

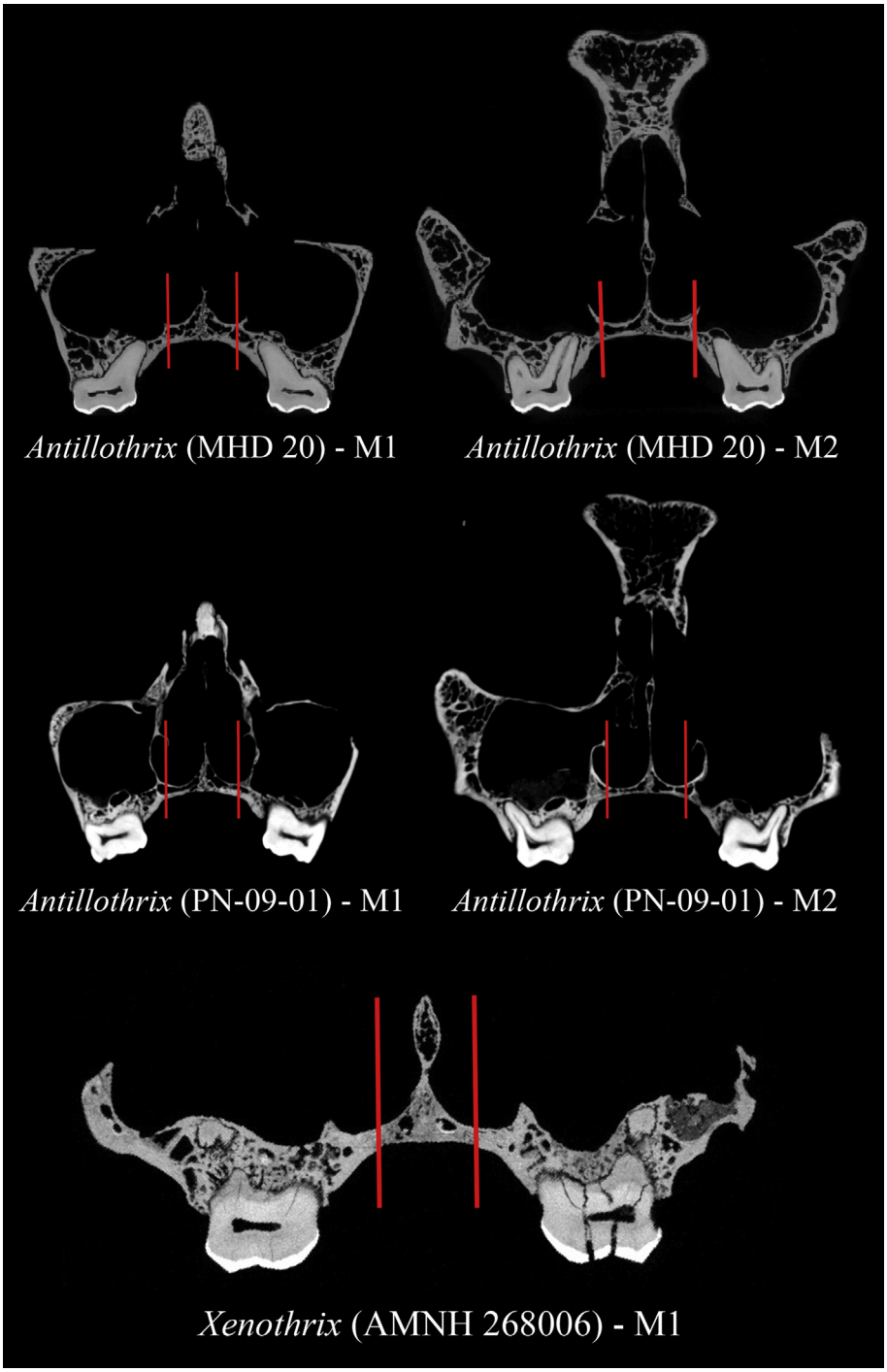

Figure 15. Nasal fossa width compared to palate width in MHD 20 (top), PN-09-01 (middle), and *Xenothrix* (bottom), shown on slices from μCT scans of the original fossil specimens (not to scale). Regardless of whether this relationship is visualized at the level of M^1 or M^2 for MHD 20 and PN-09-01, it is clear that the nasal fossa is not expanded over the borders of the palate in *Antillothrix* to the extreme degree that it is in *Xenothrix*. The bars are drawn at the approximate position of the maxillo-palatine suture to provide an anatomical standard for defining the boundaries of the palate in the same way on each specimen, as their palates and tooth rows are shaped quite differently.

pitheciins all have a C/P^4 size value over 1, and these species habitually use their canine teeth during sclerocarp foraging behaviors (Kinzey, 1992; Rosenberger, 1992). Males and females of all species of pitheciins had C/P^4 values that were significantly different from each other (unpaired t-test, $p < .05$) as did *Lagothrix*, *Alouatta*, and *Saimiri*. Importantly, for *Lagothrix*, this difference meant that females and males would likely be coded differently for this character as females had an average C/P^4 value of 0.89 while males had an average value of 1.20. While this character was evidently sexually dimorphic in the other taxa (e.g., *Pithecia, Chiropotes, Cacajao, Alouatta,* and *Saimiri)*, the difference would not have resulted in different coding for use in a cladistic character matrix as the differences did not fall over the boundary of two different character codes. For *Ateles*, *Brachyteles*, *Cebus*, *Aotus*, and *Callicebus* there was not a statistically significant difference between males and females.

The inclusion of some of the new *Antillothrix* craniodental material in more recent phylogenetic analyses has shown that the alternative scoring of these characters hitherto unknown in this taxon can challenge the idea of Caribbean monophyly, or at least lessen support for the hypothesis by failing to present corroborating synapomorphies. Kay (2015), for example, infers a monophyletic relationship between *Antillothrix* and *Paralouatta* only, to the exclusion of *Xenothrix*; all three taxa are considered stem platyrrhines with *Xenothrix* as sister taxon to the crown groups. As mentioned above, a key cranial synapomorphy of Horovitz and MacPhee's Antillean clade was the wide nasal fossa (Horovitz and MacPhee, 1999; MacPhee and Horovitz, 2004), but the new *Antillothrix* crania do not possess this trait. The same can be said for the ventrally displaced zygomatic arch that was formerly used to link all of the Caribbean taxa monophyletically to *Callicebus*. Overall, the new evidence from the MHD 20 cranium does not provide strong support for the phylogenetic conclusions drawn by previous work regarding the monophyletic relationship amongst *Antillothrix, Paralouatta*, and *Xenothrix*, or the exclusive relationship between any of those genera and *Callicebus*.

6. Conclusions

While not a formal phylogenetic analysis, the results presented here support the idea of the composite nature of the morphology of *Antillothrix* as has been discussed for the other cranial specimens, MHD 01 and PN-09-01. The MHD 20 cranium, with its elongated neurocranium, relatively large face, and vertical nuchal plane exhibits morphology reminiscent of the *Alouatta* cranium amongst extant taxa while being phenetically linked most strongly overall to the atelines *Brachyteles* and *Lagothrix*. It does not clearly exhibit any of the shared derived characters typically used to diagnose the extant platyrrhine clades. The body mass estimate of 3.2–3.3 kg based on the centroid size of the MHD 20 cranium is similar to the estimates based on craniodental dimensions of PN-09-01; both are smaller than previous body mass estimates based on teeth alone or postcranial joint sizes. While the known cranial specimens attributed to *Antillothrix* have given equivocal answers to the question of its phenetic and phylogenetic affinities, other anatomical regions are clearer. The mandible of MHD 01 has been shown to be very similar to that of the Pitheciidae while the dentition of these and several other specimens is more primitive than that seen in any of the living families, with closest resemblances to Miocene Argentine fossils. This highlights the dangers of relying on just one anatomical region or element in an analysis as well as the necessity of including as many fossil specimens as possible in a comparative sample rather than relying on the morphology of the extant genera alone to make inferences about their extinct relatives, as those taxa are all derived in their own unique ways.

Acknowledgements

We thank Director Christian Martinez of the Museo del Hombre Dominicano for facilitating our research. We are indebted to Phillip Lehman and the Dominican Republic Speleological Society for their generous and concerted efforts to recover vertebrate remains from submerged sites. This work was supported by generous funding from the NSF (NSF #0966166 NYCEP IGERT) and the Waitt Foundation/National Geographic Society (#W145-10). We would like to thank Eileen Westwig and Neil Duncan for access to specimens from the Mammalogy collections at the AMNH, Morgan Hill and Henry Towbin for support in the AMNH Microscopy and Imaging Facility, Matt Tocheri for providing the surface files for the specimens in the Smithsonian 3D digital archive, Zach Klukkert for providing surface files for many of the *Chiropotes* and *Cebus* specimens used in the comparative extant sample, Melissa Tallman, Marta Pina, and Salvador Moya-Sola for scanning and providing the surface file of the cast of the MCL 06 *Cartelles* cranium, Kari Allen for invaluable statistical troubleshooting, and Eric Delson for providing access to the cast of the MNHN V194 *Paralouatta* cranium. Dr. Tallman and several anonymous reviewers also gave very thorough and helpful comments that greatly strengthened this manuscript. Special thanks also to Ross MacPhee for access to the original AMNH 268006 *Xenothrix* palate and Rich Kay and Doug Boyer for access to the CT scan of the PN-09-01 *Antillothrix* cranium. This is NYCEP Morphometrics Group manuscript #100.

Supplementary Online Material

Supplementary online material related to this article can be found at http://dx.doi.org/10.1016/j.jhevol.2017.02.002.

References

Allen, K.L., Kay, R.F., Hunt, K.D., Beeker, C.D., Conrad, G.W., Keller, J., 2012. Brain size and endocranial morphology of *Antillothrix* (Holocene, Dominican Republic, Hispaniola). Am. J. Phys. Anthropol. S54, 82.
Aristide, L., dos Reis, S.F., Machado, A.C., Lima, I., Lopes, R.T., Perez, S.I., 2015. Encephalization and diversification of the cranial base in platyrrhine primates. J. Hum. Evol. 81, 29–40.
Aristide, L., dos Reis, S.F., Machado, A.C., Lima, I., Lopes, R.T., Perez, S.I., 2016. Brain shape convergence in the adaptive radiation of New World monkeys. Proc. Natl. Acad. Sci. 113, 2158–2163.
Arnold, C., Matthews, L.J., Nunn, C.J., 2010. The 10kTrees website: A new online resource for primate phylogeny. Evol. Anthropol. 19, 114–118.
Ashley-Montagu, M.F., 1933. The anthropological significance of the pterion in the primates. Am. J. Phys. Anthropol. 18, 159–336.
Bjarnason, A., Soligo, C., Elton, S., 2015. Phylogeny, ecology, and morphological evolution in the atelid cranium. Int. J. Primatol. 36, 513–529.
Blanchon, P., Shaw, J., 1995. Reef drowning during the last deglaciation: evidence for catastrophic sea-level rise and ice sheet collapse. Geology 23, 4–8.
Bookstein, F., 1991. Morphometric Tools for Landmark Data: Geometry and Biology. Cambridge University Press, Cambridge.
Boyer, D.M., Kaufman, S., Gunnell, G.F., Rosenberger, A.L., Delson, E., 2014. Managing 3D digital data sets of morphology: MorphoSource is a new project-based data archiving and distribution tool. Am. J. Phys. Anthropol. 153, 84.
Cooke, S.B., 2011. Paleodiet of extinct platyrrhines with emphasis on the Caribbean forms: three-dimensional geometric morphometrics of mandibular second molars. Anat. Rec. 294, 2073–2091.
Cooke, S.B., Tallman, M., 2012. New endemic platyrrhine femur from Haiti: Description and locomotor analysis. J. Hum. Evol. 63, 560–567.
Cooke, S.B., Rosenberger, A.L., Turvey, S., 2011. An extinct monkey from Haiti and the origins of the Greater Antillean primates. Proc. Natl. Acad. Sci. 108, 2699–2704.
Cooke, S.B., Mychajliw, A., Southon, J., MacPhee, R.D.E. Jamaica's last monkey: the extinction of *Xenothrix mcgregori*. J. Mammal (in press).
Delson, E., Terranova, C., Jungers, W.L., Sargis, E., Jablonski, N., Dechow, P., 2000. Body mass in Cercopithecidae (Primates, Mammalia): Estimation and scaling in extinct and extant taxa. Anthropol. Pap. Am. Mus. Nat. Hist. 83, 1–159.
Felsenstein, J., 1985. Phylogenies and the comparative method. Am. Nat. 125, 1–15.
Ford, S.M., Morgan, G.S., 1986. A new ceboid femur from the late Pleistocene of Jamaica. J. Vert. Paleontol. 6, 281–289.
Frost, S.R., Marcus, L.F., Bookstein, F.L., Reddy, D.P., Delson, E., 2003. Cranial allometry, phylogeography, and systematics of large-bodied papionins (Primates: Cercopithecinae) inferred from geometric morphometric analysis of landmark data. Anat. Rec. 275, 1048–1072.
Fulwood, E.L., Boyer, D.M., Kay, R.F., 2016. Stem members of Platyrrhini are distinct from catarrhines in at least one derived cranial feature. J. Hum. Evol. 100, 16–24.
Gladman, J.T., Rosenberger, A.L., 2013. New interpretations of the positional behaviors of the Dominican subfossil, *Antillothrix bernensis*, from the pectoral and pelvic girdles. Am. J. Phys. Anthropol. S56, 130–131.
Halenar, L.B., 2011. Reconstructing the locomotor repertoire of *Protopithecus brasiliensis* I: Body size. Anat. Rec. 294, 2024–2047.
Halenar, L.B., 2012. Paleobiology of *Protopithecus brasiliensis*, a plus-size Pleistocene platyrrhine from Brazil. Ph.D. Dissertation, City University of New York.
Halenar, L.B., 2015. Investigating the variation at pterion across platyrrhines, with special attention to *Alouatta*. Am. J. Phys. Anthropol. S60, 157.
Halenar, L.B., Rosenberger, A.L., 2013. A closer look at the "*Protopithecus*" fossil assemblages: new genus and species from Bahia, Brazil. J. Hum. Evol. 65, 374–390.
Halenar, L.B., Tallman, M., 2013. Investigating the relationship between endocranial volume and cranial shape in *Alouatta*. Am. J. Phys. Anthropol. 56, 141.
Hammer, Ø., Harper, D.A.T., Ryan, P.D., 2001. PAST: Paleontological statistics software package for education and data analysis. Palaeontologia Electronica 4, 1–9.

Hartwig, W., Rosenberger, A.L., Norconk, M.A., Young Owl, M., 2011. Relative brain size, gut size, and evolution in New World monkeys. Anat. Rec. 294, 2207–2221.
Hartwig, W.C., Cartelle, C., 1996. A complete skeleton of the giant South American primate *Protopithecus*. Nature 381, 307–311.
Hershkovitz, P., 1977. Living New World Monkeys (Platyrrhini), Vol. 1. University of Chicago Press, Chicago.
Hershkovitz, P., 1988. The subfossil monkey femur and subfossil monkey tibia of the Antilles: a review. Int. J. Primatol. 9, 365–384.
Higuera-Gundy, A., Brenner, M., Hodell, D.A., Curtis, J.H., Leyden, B.W., Binford, M.W., 1999. A 10,300 14C yr record of climate and vegetation change from Haiti. Quatern. Res. 52, 159–170.
Horovitz, I., 1997. Platyrrhine systematics and the origin of Greater Antilles monkeys. Ph.D. Dissertation, State University of New York at Stony Brook.
Horovitz, I., MacPhee, R.D.E., 1999. The quaternary Cuban platyrrhine *Paralouatta varonai* and the origin of Antillean monkeys. J. Hum. Evol. 36, 33–68.
Isler, K., Kirk, E.C., Miller, J.M.A., Albrecht, G.A., Gelvin, B.R., Martin, R.D., 2008. Endocranial volumes of primate species: scaling analyses using a comprehensive and reliable data set. J. Hum. Evol. 55, 967–978.
Jungers, W.L., Demes, B., Godfrey, L.R., 2008. How big were the "giant" extinct lemurs of Madagascar? In: Fleagle, J.G., Gilbert, C.C. (Eds.), Elwyn Simons: a Search for Origins. Springer, New York, pp. 343–360.
Kay, R.F., 2015. Biogeography in deep time–What do phylogenetics, geology, and paleoclimate tell us about early platyrrhine evolution? Mol. Phylogenet. Evol. 82, 358–374.
Kay, R.F., Fleagle, J.G., Mitchell, T.R.T., Colbert, M.W., Brown, T.M., Powers, D.W., 2008. The anatomy of *Dolichocebus gaimanensis*, a primitive platyrrhine monkey from Argentina. J. Hum. Evol. 54, 323–382.
Kay, R.F., Allen, K., Gonzales, L., Krueger, K., 2011a. Dietary reconstruction of *Antillothrix bernensis*, a Holocene monkey from the Dominican Republic. J. Vert. Paleontol. Supplement 31, 135.
Kay, R.F., Hunt, K.D., Beeker, C.D., Conrad, G.W., Johnson, C.C., Keller, J., 2011b. Preliminary notes on a newly discovered skull of the extinct monkey *Antillothrix* from Hispaniola and the origin of the Greater Antillean monkeys. J. Hum. Evol. 60, 124–128.
Kinzey, W., 1992. Dietary and dental adaptations in the Pitheciinae. Am. J. Phys. Anthropol. 88, 499–514.
MacPhee, R.D.E., Fleagle, J.G., 1991. Postcranial remains of *Xenothrix mcgregori* (Primates, Xenotrichidae) and other late Quaternary mammals from Long Mile Cave, Jamaica. Bull. Am. Mus. Nat. Hist. 206, 287–321.
MacPhee, R.D.E., Horowitz, I., 2002. Extinct Quaternary platyrrhines of the Greater Antilles and Brazil. In: Hartwig, W. (Ed.), The Primate Fossil Record. Cambridge University Press, New York, pp. 189–200.
MacPhee, R.D.E., Horovitz, I., 2004. New craniodental remains of the Quaternary Jamaican monkey *Xenothrix mcgregori* (Xenotrichini, Callicebinae, Pitheciidae), with a reconsideration of the *Aotus* hypothesis. Am. Mus. Novit. 3434, 1–55.
MacPhee, R.D.E., Meldrum, J., 2006. Postcranial remains of the extinct monkeys of the Greater Antilles, with evidence for semiterrestriality in *Paralouatta*. Am. Mus. Novit. 3516, 1–65.
MacPhee, R.D.E., Woods, C., 1982. A new fossil cebine from Hispaniola. Am. J. Phys. Anthropol. 58, 419–436.
MacPhee, R.D.E., Horovitz, I., Arredondo, O., Vasquez, O.J., 1995. A new genus for the extinct Hispaniolan monkey *Saimiri bernensis* Rímoli, 1977, with notes on its systematic position. Am. Mus. Novit. 3134, 1–21.
MacPhee, R.D.E., Iturralde-Vinent, M.A., Gaffney, E.S., 2003. Domo de Zaza, an early Miocene vertebrate locality in south-central Cuba, with notes on the tectonic evolution of Puerto Rico and the Mona Passage. Am. Mus. Novit. 3394, 1–42.
McFarlane, D.A., Lundberg, J., Fincham, A.G., 2002. A late Quaternary paleoecological record from caves of southern Jamaica, West Indies. J. Cave Karst Studies 64, 117–125.
Miller, G.S., 1929. Mammals eaten by Indians, owls, and Spaniards in the coast region of the Dominican Republic. Smithson. Misc. Coll. 82, 1–16.
Mitteroecker, P., Bookstein, F., 2011. Linear discrimination, ordination, and the visualization of selection gradients in modern morphometrics. Evol. Biol. 38, 100–114.
O'Higgins, P., Jones, N., 1998. Facial growth in *Cercocebus torquatus*: an application of three-dimensional geometric morphometric techniques to the study of morphological variation. J. Anat. 193, 251–272.
O'Higgins, P., Jones, N., 2006. Morphologika2. The Hull York Medical School, Heslington: Functional Morphology and Evolution Research Group.
Orme, D., Freckleton, R., Thomas, G., Petzoldt, T., Fritz, S., Isaac, N., Pearse, W., 2010. Caper: Comparative Analyses of Phylogenetics and Evolution in R. R package version 0.4/r71.
Perelman, P., Johnson, W.E., Roos, C., Seuánez, H.N., Horvath, J.E., Moreira, M.A., Kessing, B., Pontius, J., Roelke, M., Rumpler, Y., Schneider, M.P.C., Silva, R., O'Brien, S.J., Recon-Slattery, J., 2011. A molecular phylogeny of living primates. PLoS Genet. 7, e1001342.
Perez, S.I., Klaczko, J., Rocatti, G., dos Reis, S.F., 2011. Patterns of cranial shape diversification during the phylogenetic branching process of New World monkeys (Primates: Platyrrhini). J. Evolution. Biol. 24, 1826–1835.
Perry, J.M., Cooke, S.B., Halenar, L.B., Runestad, J.A., Ruff, C.B., 2015. Body mass estimation in platyrrhines: methodological considerations and fossil application. Am. J. Phys. Anthropol. S60, 251.
Rímoli, R., 1977. A new species of monkey (Cebidae: Saimirinae: *Saimiri*) from Hispaniola (original title in Spanish). Cuadernos de CENDIA, Universidad Autónoma de Santa Domingo 242, 5–14.
Rivero, M., Arredondo, O., 1991. *Paralouatta varonai*, a new Quaternary platyrrhine from Cuba. J. Hum. Evol. 21, 1–11.
Rosenberger, A.L., 1977. *Xenothrix* and ceboid phylogeny. J. Hum. Evol. 6, 461–481.
Rosenberger, A.L., 1978. New species of Hispaniolan monkey: A comment. Anuario Cientifico. Universidad Cent. Este. 3, 249–251.
Rosenberger, A.L., 1992. Evolution of feeding niches in New World monkeys. Am. J. Phys. Anthropol. 88, 525–562.
Rosenberger, A.L., 2002. Platyrrhine paleontology and systematics: the paradigm shifts. In: Hartwig, W. (Ed.), The Primate Fossil Record. Cambridge University Press, New York, pp. 151–159.
Rosenberger, A.L., Cooke, S.B., Rímoli, R., Ni, X., Cardosa, L., 2011. First skull of *Antillothrix bernensis*, an extinct relict monkey from the Dominican Republic. P. Roy. Soc. B. 278, 67–74.
Rosenberger, A.L., Klukkert, Z., Cooke, S.B., Rímoli, R., 2013. Rethinking *Antillothrix*: The mandible and its implications. Am. J. Primatol. 75, 825–836.
Rosenberger, A.L., Pickering, R., Green, H., Cooke, S.B., Tallman, M., Morrow, A., Rímoli, R., 2015a. 1.32 ± 0.11 Ma age for underwater remains constrain antiquity and longevity of the Dominican primate *Antillothrix bernensis*. J. Hum. Evol. 88, 85–96.
Rosenberger, A.L., Cooke, S.B., Halenar, L.B., Tejedor, M.F., Hartwig, W.C., Novo, N.M., Muñoz-Saba, Y., 2015b. Fossil alouattines and the origins of *Alouatta*: Craniodental diversity and interrelationships. In: Kowalewski, M., Garber, P., Cortes-Ortiz, L., Urbani, B., Youlatos, D. (Eds.), Howler Monkeys: Adaptive Radiation, Systematics, and Morphology. Springer, New York, pp. 21–54.
Sears, K., Finarelli, J., Flynn, J.J., Wyss, A.R., 2008. Estimating body mass in New World "monkeys" (Platyrrhini, Primates), with a consideration of the Miocene platyrrhine, *Chilicebus carrascoensis*. Am. Mus. Novit. 3617, 1–29.
Shearer, B.M., Tallman, M., Cooke, S.B., Halenar, L.B., Reber, S.L., Plummer, J., Delson, E., 2014. Evaluating causes of error in landmark-based data collection using scanners. Am. J. Phys. Anthropol. S58, 237.
Smith, R.J., 1993. Bias in equations used to estimate fossil primate body mass. J. Hum. Evol. 25, 31–41.
Tallman, M., Cooke, S.B., 2016. New endemic platyrrhine humerus from Haiti and the evolution of the Greater Antillean platyrrhines. J. Hum. Evol. 91, 144–166.
Wiley, D.F., Amenta, N., Alcantara, D.A., Ghosh, D., Kil, Y.J., Delson, E., Harcourt-Smith, W., Rohlf, F.J., St. John, K., Hamann, B., 2005. Evolutionary morphing. Proc. IEEE Vis. 2005, 431–438.
Williams, E.E., Koopman, K.F., 1952. West Indian fossil monkeys. Am. Mus. Novit. 1546, 1–16.
Yokoyama, Y., Lambeck, K., De Deckker, P., Johnston, P., Fifield, L.K., 2000. Timing of the Last Glacial Maximum from observed sea-level minima. Nature 406, 713–716.